

ECOLE POLYTECHNIQUE

CENTRE DE MATHÉMATIQUES APPLIQUÉES

UMR CNRS 7641

91128 PALAISEAU CEDEX (FRANCE). Tél: 01 69 33 41 50. Fax: 01 69 33 30 11

<http://www.cmap.polytechnique.fr/>

**DETAILED MODELING OF PLANAR
TRANSCRITICAL H₂-O₂-N₂ FLAMES**

Vincent Giovangigli, Lionel Matuszewski,
and Francis Dupoirieux

R.I. 688

Juillet 2010

Detailed modeling of planar transcritical H₂-O₂-N₂ flames

Vincent Giovangigli^a, Lionel Matuszewski^{b*}, *and Francis Dupoirieux^b

^a*CMAP-CNRS, Ecole polytechnique, Palaiseau, France;*

^b*ONERA DEFA, 6 chemin de la Hunière, Palaiseau, France*

Abstract

We first investigate a detailed high pressure flame model. Our model is based on thermodynamics of irreversible processes, statistical thermodynamics, and the kinetic theory of dense gases. We study thermodynamic properties, chemical production rates, transport fluxes, and establish that entropy production is nonnegative. We next investigate the structure of planar transcritical H₂-O₂-N₂ flames and perform a sensitivity analysis with respect to the model. Nonidealities in the equation of state and in the transport fluxes have a dramatic influence on the cold zone of the flame. Nonidealities in the chemical production rates—consistent with thermodynamics and important to insure positivity of entropy production—may also strongly influence flame structures at very high pressures. At sufficiently low temperatures, fresh mixtures of H₂-O₂-N₂ flames are found to be thermodynamically unstable in agreement with experimental results. We finally study the influence of various parameters associated with the initial reactants on the structure of transcritical planar H₂-O₂-N₂ flames as well as lean and rich extinction limits.

1 Introduction

Progresses in the efficiency of automotive engines, gas turbines and rocket motors have notably been achieved with high pressure combustion. Many experimental and theoretical studies have thus been devoted to combustion processes at high pressure. In particular, laminar flames have been investigated experimentally by Schilling and Franck [1] and turbulent flames by Chehroudi et. al. [2], Habiballah et al. [3] and Candel et al. [4]. Numerical simulations of high pressure planar flames have been performed by El Gamal et al. [5], mixing layers by Okongo and Bellan [9], counterflow laminar flames by Saur et al. [6], Ribert et al. [7], and Pons et al. [8], and turbulent flames by Zong and Yang [10], and Bellan [11]. More recent research involves supercritical combustion of oxygen in industrial configurations as studied by Oefelein [12], Zong and Yang [13], and Schmitt et al. [14].

In this paper, we first investigate a detailed high pressure flame model. Our dense fluid model is based on thermodynamics of irreversible processes [15, 16, 17, 18], statistical mechanics [19, 20, 21], statistical thermodynamics [22], as well as the kinetic theory of dense gases [23, 24, 25]. We discuss in particular thermodynamic properties, chemical production rates, transport fluxes, as well as thermochemistry and transport coefficients.

Thermodynamics is built as usual from the pressure law by assuming a Gibbsian structure and compatibility with perfect gases at low densities [26, 27, 28]. The nonideal chemical production rates that we consider are deduced from statistical thermodynamics [22] and are compatible with the symmetric forms of rates of progress derived from the kinetic theory of dilute reactive gases [29, 30]. The transport fluxes are also deduced from various macroscopic or molecular theories [16, 17, 18, 22, 23, 24, 25]. The transport coefficients are finally obtained by using classical correlations as well as Stefan-Maxwell equations derived from the kinetic theory of dense gases [25] or from experiments in fluids [31]. We also discuss thermochemistry coefficients, in particular

**Corresponding author. Email: lionel.matuszewski@onera.fr

for chemically unstable species for which critical states do not exist so that applying the principle of equivalent states does not make sense a priori. The resulting theoretical flame model is shown to satisfy the second principle of thermodynamics, that is, entropy production due to transport fluxes and chemistry are both shown to be nonnegative.

The high pressure flame model is then used to investigate H₂-O₂-N₂ planar flames. Planar flames are important from a theoretical point of view but are also the basis of numerous turbulent combustion models [32, 33]. We first establish that, at sufficiently low temperatures, fresh mixtures of H₂-O₂-N₂ are thermodynamically unstable. These mixtures split between a hydrogen-rich gaseous-like phase and a hydrogen-poor liquid-like phase in agreement with experimental results [34, 35]. We next discuss the structure of transcritical flames for thermodynamically stable fresh mixtures of H₂-O₂-N₂ and perform a comprehensive sensitivity analysis with respect to the model. Real gases thermodynamics is found to be of fundamental importance to correctly represent the fluids under consideration. The influence of transport nonidealities is also critical in the cold part of the flame in order to prevent unrealistic hydrogen diffusion from dense fresh gases into the flame front. The dependence of thermal conductivity on density has an important impact on flame structures. We further show that the chemical production rates nonidealities, which are consistent with thermodynamics and insure the positivity of entropy production, may dramatically modify flame structures at very high pressure, although their influence is still weak around $p = 100$ atm.

We finally investigate the influence of various parameters, like the equivalence ratio φ or the fresh gas temperature T^{fr} , on the structure of planar transcritical H₂-O₂-N₂ flames. We establish in particular that, in the parameter plane (φ, T^{fr}) , the flammability domain is bounded on the left by the lean extinction limit, on the right by the rich extinction limit, and at the bottom by the thermodynamic stability limit of the incoming fresh mixture.

The detailed flame model is presented in Sections 2 and 3. Computational considerations are addressed in Section 4 and the thermodynamic stability of fresh mixtures is investigated in Section 5. Planar transcritical H₂-O₂-N₂ flame structures are analyzed in Section 6 and the dependence on fresh mixtures parameters is addressed in Section 7.

2 Theoretical formulation

In this section we investigate a detailed high pressure flame model and establish that the corresponding entropy production is nonnegative. When pressure is increasing in a fluid, molecules stay longer in mutual interaction during collisions and the fluid macroscopic behavior may change continuously from that of a dilute gas to that of a liquid. Our dense fluid model is derived from macroscopic theories like thermodynamics of irreversible processes [15, 16, 17, 18] and statistical thermodynamics [22], as well as molecular theories like statistical mechanics [19, 20, 21] and the kinetic theory of dense gases [24, 25]. The relations expressing the various system coefficients are detailed in Section 3.

2.1 Conservation equations

The one-dimensional steady conservation equations for species mass and energy in a dense fluid—under the small Mach number limit—are in the form

$$m Y_i' + \mathcal{F}_i' = m_i \omega_i, \quad i \in \mathcal{S}, \quad (1)$$

$$m h' + q' = 0, \quad (2)$$

where $m = \rho u$ denotes the mass flow rate, ρ the mass density, u the fluid normal velocity, the superscript $'$ the derivation with respect to the spatial coordinate x , Y_i the mass fraction of the i th species, \mathcal{F}_i the diffusion flux of the i th species, m_i the molar mass of the i th species, ω_i the molar production rate of the i th species, $\mathcal{S} = \{1, \dots, n^e\}$ the species indexing set, n^e the number

of species, h the enthalpy per unit mass of the mixture, and q the heat flux. The momentum equation uncouples from (1)(2) and may only be used to evaluate the perturbed pressure as for dilute gases [30].

The boundary conditions at the origin are naturally written in the form [36, 37]

$$m(Y_i(0) - Y_i^{\text{fr}}) + \mathcal{F}_i(0) = 0, \quad i \in \mathcal{S}, \quad (3)$$

$$m(h(0) - h^{\text{fr}}) + q(0) = 0, \quad (4)$$

where the superscript ^{fr} refers to the fresh mixture. The downstream boundary conditions are in the form

$$Y'_i(+\infty) = 0, \quad i \in \mathcal{S}, \quad T'(+\infty) = 0, \quad (5)$$

and the translational invariance of the model is removed by imposing a given temperature T^{fx} at a given arbitrary point x^{fx} of $[0, \infty)$

$$T(x^{\text{fx}}) - T^{\text{fx}} = 0, \quad (6)$$

where T denotes the absolute temperature. These boundary and internal conditions (3)–(6) have first been used by Sermange [36] for $x^{\text{fx}} \neq 0$ whereas $x^{\text{fx}} = 0$ was first chosen in reference [37]. The relations expressing the thermodynamic properties like h , the transport fluxes \mathcal{F}_i , $i \in \mathcal{S}$, and q , and the chemical production rates ω_i , $i \in \mathcal{S}$, are investigated in the next sections.

2.2 Thermodynamics properties

Various equations of state have been introduced to represent the behavior of dense fluids [38, 39, 40, 41, 42, 6, 43]. The Benedict-Webb-Rubin equation of state [38] and its modified form by Soave [39] are notably accurate but are mathematically uneasy to handle. On the other hand, the Soave-Redlich-Kwong equation of state [40, 41] and the Peng-Robinson equation of state [42] yield less accuracy but allow an easier inversion by using Cardan's formula thanks to their cubic form. Statistical mechanics [19] and the kinetic theory of dense gases [25] have similarly suggested equations of state in polynomial form with respect to the density.

In this study, we have used the Soave-Redlich-Kwong equation of state [40, 41]

$$p = \sum_{i \in \mathcal{S}} \frac{Y_i}{m_i} \frac{RT}{v - b} - \frac{a}{v(v + b)}, \quad (7)$$

where p denotes the pressure, R the perfect gas constant, $v = 1/\rho$ the volume per unit mass, and a and b the massic attractive and repulsive parameters, respectively. These parameters $a(Y_1, \dots, Y_{n^e}, T)$ and $b(Y_1, \dots, Y_{n^e})$ are evaluated with the usual Van der Waals mixing rules written here with a massic formulation

$$a = \sum_{i,j \in \mathcal{S}} Y_i Y_j \sqrt{a_i a_j}, \quad b = \sum_{i \in \mathcal{S}} Y_i b_i. \quad (8)$$

The pure-component parameters $a_i(T)$ and b_i are deduced from the corresponding macroscopic fluid behavior or from interaction potentials as discussed in Section 3. The validity of this equation of state (7) and of the corresponding mixing rules (8) have been carefully studied by comparison with NIST data by Congiunti et al. [44] and with results of Monte Carlo simulations by Colonna and Silva [45] and Cañas-Marín et al. [46, 47]. Moreover, this equation of state has already been used in high pressure combustion models by Meng and Yang [48] and Ribert et al. [7].

Once a pressure law is given, there exists a unique corresponding Gibbsian thermodynamics compatible at low densities with that of perfect gases [28, 49]. There are limitations on the pressure law $p = p(v, Y_1, \dots, Y_{n^e}, T)$ for such a construction, that is, p must be zero homogeneous with respect to the variable (v, Y_1, \dots, Y_{n^e}) and the entropy Hessian matrices of the corresponding Gibbsian thermodynamics must be negative semi-definite [49].

For the Soave-Redlich-Kwong equation of state it is further possible to evaluate analytically the corresponding thermodynamic properties. The real-gas free energy per unit mass $f = f(v, Y_1, \dots, Y_{n^e}, T)$ can be written for instance

$$f = \sum_{i \in \mathcal{S}} Y_i f_i^{\text{PG}\star} + \sum_{i \in \mathcal{S}} \frac{Y_i}{m_i} RT \ln \left(\frac{Y_i RT}{m_i (v - b) p^{\text{st}}} \right) - \frac{a}{b} \ln \left(1 + \frac{b}{v} \right), \quad (9)$$

where $f_i^{\text{PG}\star} = f_i^{\text{PG}\star}(T)$ is the perfect-gas free energy per unit mass of the i th species at the standard pressure p^{st} . The perfect gas properties are evaluated as usual from relations like

$$f_i^{\text{PG}\star} = e_i^{\text{st}} + \int_{T^{\text{st}}}^T c_{vi}^{\text{PG}}(\tau) d\tau - T \left(s_i^{\text{st}} + \int_{T^{\text{st}}}^T \frac{c_{vi}^{\text{PG}}(\tau) + r_i}{\tau} d\tau \right), \quad (10)$$

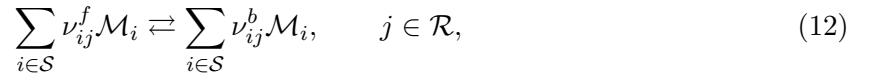
where e_i^{st} and s_i^{st} are the formation energy and entropy at standard temperature T^{st} and pressure p^{st} of the i th species, respectively, c_{vi}^{PG} the perfect gas specific heat at constant volume of the i th species, and $r_i = R/m_i$ the specific gas constant of the i th species. Other thermodynamic properties may be evaluated as well and more details are presented in Appendix A. In the following, we will need in particular the real gas Gibbs function of the i th species g_i and the corresponding molar dimensionless chemical potentials μ_i , $i \in \mathcal{S}$, defined by

$$\mu_i = \frac{m_i g_i}{RT}, \quad i \in \mathcal{S}. \quad (11)$$

According to Beattie [27], Van der Waals has been the first to derive thermodynamic properties of real gases by using a high pressure equation of state and matching with perfect gases, but he did not eliminate improper integrals in the expressions of entropy [27], and Gillespie [26] has been the first to properly compute the entropy and fugacity of a gas mixture at high pressure by these techniques [27].

2.3 Chemical production rates

We consider an arbitrary complex reaction mechanism with n^r reactions involving n^e species which may be written symbolically



where ν_{ij}^f and ν_{ij}^b denote the forward and backward stoichiometric coefficients of the i th species in the j th reaction, \mathcal{M}_i the symbol of the i th species, and $\mathcal{R} = \{1, \dots, n^r\}$ the reaction indexing set. The molar production rate of the i th species ω_i is then given by [22]

$$\omega_i = \sum_{j \in \mathcal{R}} (\nu_{ij}^b - \nu_{ij}^f) \tau_j, \quad (13)$$

where τ_j denotes the rate of progress of the j th reaction. The proper form for the rate of progress of the j th reaction τ_j is deduced from statistical thermodynamics [22]

$$\tau_j = \kappa_j^s \left(\exp \left(\sum_{i \in \mathcal{S}} \nu_{ij}^f \mu_i \right) - \exp \left(\sum_{i \in \mathcal{S}} \nu_{ij}^b \mu_i \right) \right), \quad (14)$$

where κ_j^s is the symmetric reaction constant of the j th reaction. This form for rates of progress—which does not seem to have previously been used—insures that entropy production due to chemical reactions is nonnegative, coincides with the ideal gas rate in the perfect gas limit and is compatible with traditional nonidealities used to estimate *equilibrium constants*.

In the perfect gas limit, we indeed recover the ideal gas rate of progress of the j th reaction τ_j^{PG} given by

$$\tau_j^{\text{PG}} = \kappa_j^f \prod_{i \in \mathcal{S}} (\gamma_i^{\text{PG}})^{\nu_{ij}^f} - \kappa_j^b \prod_{i \in \mathcal{S}} (\gamma_i^{\text{PG}})^{\nu_{ij}^b}, \quad (15)$$

where κ_j^f and κ_j^b denote the forward and backward reaction constants of the j th reaction, respectively, $\gamma_i^{\text{PG}} = Y_i/(v^{\text{PG}}m_i) = x_i p/RT$ the perfect gas molar concentration of the i th species, $v^{\text{PG}} = RT/mp$ the perfect gas massic volume, $x_i = Y_i m/m_i$, $i \in \mathcal{S}$, the species mole fractions, m the molar mass of the mixture defined as in Appendix A, and where the superscript PG refers to ideal solutions of perfect gases. The reaction constants κ_j^f and κ_j^b are related through the ideal gas equilibrium constant $\kappa_j^{\text{eq,PG}}$ of the j th reaction

$$\kappa_j^f = \kappa_j^b \kappa_j^{\text{eq,PG}}, \quad \kappa_j^{\text{eq,PG}} = \exp\left(\sum_{i \in \mathcal{S}} (\nu_{ij}^f - \nu_{ij}^b) \mu_i^{\text{u,PG}}\right), \quad (16)$$

where $\mu_i^{\text{u,PG}}$ denotes the perfect gas reduced chemical potential of the i th species at unit concentration. This standard potential is given by

$$\mu_i^{\text{u,PG}} = \frac{m_i g_i^{\text{PG*}}(T)}{RT} + \ln\left(\frac{RT}{p^{\text{st}}}\right), \quad (17)$$

where $g_i^{\text{PG*}}$ denotes the perfect gas specific Gibbs function of the i th species at the standard pressure p^{st} . The perfect gas dimensionless potential $\mu_i^{\text{PG}} = m_i g_i^{\text{PG}}/RT$, where g_i^{PG} is the perfect gas Gibbs function of the i th species, is then given by $\mu_i^{\text{PG}} = \mu_i^{\text{u,PG}} + \ln \gamma_i^{\text{PG}}$. Defining the symmetric constant κ_j^s of the j th reaction by

$$\kappa_j^s = \kappa_j^f \exp\left(-\sum_{i \in \mathcal{S}} \nu_{ij}^f \mu_i^{\text{u,PG}}\right) = \kappa_j^b \exp\left(-\sum_{i \in \mathcal{S}} \nu_{ij}^b \mu_i^{\text{u,PG}}\right), \quad (18)$$

we then recover the ideal gas rate of progress (15) from the symmetric form (14) and from the relations $\mu_i^{\text{PG}} = \mu_i^{\text{u,PG}} + \ln \gamma_i^{\text{PG}}$, $i \in \mathcal{S}$. Identification of both forms for rates of progress (18) also yields a method for estimating the symmetric reaction constants κ_j^s , $j \in \mathcal{R}$.

The nonideal rates of progress derived from statistical thermodynamics (14) may equivalently be obtained by defining the activity coefficient a_i of the i th species

$$a_i = \exp(\mu_i - \mu_i^{\text{u,PG}}), \quad (19)$$

and by replacing γ_i^{PG} by a_i in the classical form of the rates of progress (15), keeping in mind that in the ideal gas limit we have $\gamma_i^{\text{PG}} = \exp(\mu_i^{\text{PG}} - \mu_i^{\text{u,PG}})$, $i \in \mathcal{S}$.

Various intermediate forms for rates of progress are discussed in Section 4 and investigated in Section 6. Note that changing only the equilibrium constant by taking into account nonidealities while keeping an ideal gas form (15) for either the direct or the reverse reaction rates is *inconsistent*.

To the authors' knowledge, the symmetric expression for the rates of progress in nonideal gas mixtures has first been written by Keizer [22] in the framework of statistical thermodynamics. For ideal gas mixtures, it corresponds to the usual law of mass action and may also be derived from the kinetic theory of dilute reactive gases [29, 30]. It is interesting to note that neither the ideal gas rates of progress (15) nor a fortiori the nonideal rates (14) may be derived in the framework of Onsager irreversible thermodynamics which only yields linear relations for rates of progress in terms of affinities [16, 17, 18] instead of exponential expressions.

2.4 Transport fluxes

The transport fluxes in a dense fluid mixture can be derived from thermodynamics of irreversible processes [16, 17, 18], statistical mechanics, [20, 21], statistical thermodynamics [22], as well as the kinetic theory of dense gases [24, 25]. In a one dimensional framework, and in the absence of forces acting on the species, the corresponding mass and heat fluxes are in the form

$$\mathcal{F}_i = -\sum_{j \in \mathcal{S}} L_{ij} \left(\frac{g_j}{T}\right)' - L_{iq} \left(-\frac{1}{T}\right)', \quad i \in \mathcal{S}, \quad (20)$$

$$q = -\sum_{j \in \mathcal{S}} L_{qj} \left(\frac{g_j}{T}\right)' - L_{qq} \left(-\frac{1}{T}\right)', \quad (21)$$

where L_{ij} , $i, j \in \mathcal{S} \cup \{q\}$, are the phenomenological coefficients. The transport coefficient matrix L defined by

$$L = \begin{pmatrix} L_{11} & \cdots & L_{1n^e} & L_{1q} \\ \vdots & \ddots & \vdots & \vdots \\ L_{n^e 1} & \cdots & L_{n^e n^e} & L_{n^e q} \\ L_{q1} & \cdots & L_{qn^e} & L_{qq} \end{pmatrix}, \quad (22)$$

is then symmetric positive semi-definite and has nullspace $N(L) = \mathbb{R}\mathcal{U}$, where $\mathcal{U} \in \mathbb{R}^{n^e+1}$ and $\mathcal{U} = (1, \dots, 1, 0)^t$. Since $\mu_j = m_j g_j / RT$, $j \in \mathcal{S}$, we deduce from Gibbs' relation that $d\mu_j = \frac{m_j v_j}{RT} dp + \sum_{l \in \mathcal{S}} \partial_{x_l} \mu_j dx_l - \frac{m_j h_j}{RT^2} dT$, where x_j denotes the mole fraction of the j th species, h_j the enthalpy per unit mass of the j th species, v_j the partial volume per unit mass of the j th species, and d the total differential operator. We may thus introduce the gradient of μ_j at constant temperature $(\mu_j)'_T$ and the generalized diffusion driving force $d_j = x_j (\mu_j)'_T$ in such a way that

$$x_j \mu'_j = d_j - \frac{x_j m_j h_j}{RT^2} T', \quad j \in \mathcal{S}, \quad (23)$$

and d_j may be written

$$d_j = \frac{x_j m_j v_j}{RT} p' + \sum_{l \in \mathcal{S}} \Gamma_{jl} x'_l, \quad j \in \mathcal{S}, \quad (24)$$

where $\Gamma_{jl} = x_j \partial_{x_l} \mu_j$, $j, l \in \mathcal{S}$. For isobaric planar flames, the generalized diffusion driving force d_j reduces to $d_j = \sum_{l \in \mathcal{S}} \Gamma_{jl} x'_l$, and, for perfect gases, letting $\sum_{l \in \mathcal{S}} x_l = 1$ we recover the usual formula $d_j^{\text{PG}} = x'_j$ and Γ^{PG} reduces to the identity matrix. Using the diffusion driving forces d_j , $j \in \mathcal{S}$, the transport fluxes are then rewritten in the form

$$\mathcal{F}_i = - \sum_{j \in \mathcal{S}} \frac{\hat{L}_{ij} R}{x_j m_j} d_j - \frac{\hat{L}_{iq} R}{T^2} T', \quad i \in \mathcal{S}, \quad (25)$$

$$q - \sum_{i \in \mathcal{S}} h_i \mathcal{F}_i = - \sum_{j \in \mathcal{S}} \frac{\hat{L}_{qj} R}{x_j m_j} d_j - \frac{\hat{L}_{qq} R}{T^2} T', \quad (26)$$

where the modified transport coefficients matrix \hat{L} is given by $\hat{L} = A^t L A$ with

$$\hat{L} = \begin{pmatrix} \hat{L}_{11} & \cdots & \hat{L}_{1n^e} & \hat{L}_{1q} \\ \vdots & \ddots & \vdots & \vdots \\ \hat{L}_{n^e 1} & \cdots & \hat{L}_{n^e n^e} & \hat{L}_{n^e q} \\ \hat{L}_{q1} & \cdots & \hat{L}_{qn^e} & \hat{L}_{qq} \end{pmatrix}, \quad A = \begin{pmatrix} & & & -h_1 \\ & \mathbb{I}_{n^e} & & \vdots \\ & & & -h_{n^e} \\ 0 & \cdots & 0 & 1 \end{pmatrix}, \quad (27)$$

and \mathbb{I}_{n^e} denotes the identity matrix in \mathbb{R}^{n^e} . Since $\hat{L} = A^t L A$, the matrix \hat{L} is symmetric positive semi-definite and has nullspace $N(\hat{L}) = \mathbb{R}\mathcal{U}$. Thanks to the properties $\sum_{j \in \mathcal{S}} \hat{L}_{ij} = 0$, $i \in \mathcal{S}$, and $\sum_{j \in \mathcal{S}} \hat{L}_{qj} = 0$, the transport fluxes may also easily be rewritten in terms of the linearly dependent generalized diffusion driving forces $\tilde{d}_j = d_j - Y_j \sum_{l \in \mathcal{S}} d_l$. When the forces per unit mass acting on the species are species independent—as for gravity—the corresponding terms are proportional to the mass fractions and are automatically eliminated from the linearly dependent diffusion driving forces and thus from transport fluxes.

The expressions (25)(26) for transport fluxes allow the identification of the coefficients of \hat{L} with generalized diffusion coefficients D_{ij} , $i, j \in \mathcal{S}$, thermal diffusion coefficients θ_i , $i \in \mathcal{S}$, and partial thermal conductivity $\hat{\lambda}$, by defining [25]

$$\frac{\hat{L}_{ij} R}{\rho Y_i Y_j m} = D_{ij}, \quad i, j \in \mathcal{S}, \quad \frac{\hat{L}_{iq} R}{T} = \rho Y_i \theta_i, \quad \frac{\hat{L}_{qq} R}{T^2} = \hat{\lambda}. \quad (28)$$

These symmetric multicomponent diffusion coefficients D_{ij} , $i, j \in \mathcal{S}$, introduced by Kurochkin [25], generalize the symmetric coefficients introduced for dilute gases by Waldmann [50, 51, 52]. These coefficients (28) satisfy the natural symmetry relations $D_{ij} = D_{ji}$, $i, j \in \mathcal{S}$, the mass conservation constraints $\sum_{j \in \mathcal{S}} D_{ij} Y_j = 0$, $i \in \mathcal{S}$, $\sum_{i \in \mathcal{S}} \theta_i Y_i = 0$, and the matrix D is positive semi-definite with $N(D) = \mathbb{R}y$ where $y = (Y_1, \dots, Y_{n^e})^t$ is the mass fraction vector. On the contrary, Hirschfelder, Curtiss, and Bird have artificially destroyed the natural symmetries of transport models as discussed by Van de Ree [51]. Using the generalized diffusion coefficients D_{ij} , $i, j \in \mathcal{S}$, thermal diffusion coefficients θ_i , $i \in \mathcal{S}$, and partial thermal conductivity $\hat{\lambda}$, the fluxes (25)(26) are rewritten in the familiar form

$$\mathcal{F}_i = - \sum_{j \in \mathcal{S}} \rho Y_i D_{ij} d_j - \rho Y_i \theta_i (\ln T)', \quad i \in \mathcal{S}, \quad (29)$$

$$q = \sum_{i \in \mathcal{S}} h_i \mathcal{F}_i - \frac{\rho R T}{m} \sum_{j \in \mathcal{S}} \theta_j d_j - \hat{\lambda} T'. \quad (30)$$

An alternative form—similar to that of dilute gases—is also possible by introducing the generalized thermal diffusion ratios χ_i , $i \in \mathcal{S}$, and the thermal conductivity λ defined by [16, 25, 52]

$$\theta_i = \sum_{j \in \mathcal{S}} D_{ij} \chi_j, \quad \sum_{j \in \mathcal{S}} \chi_j = 0, \quad \lambda = \hat{\lambda} - \frac{\rho R}{m} \sum_{i, j \in \mathcal{S}} D_{ij} \chi_i \chi_j. \quad (31)$$

The transport linear system defining the thermal diffusion ratios is easily shown to be well posed [65] and the transport fluxes can be rewritten

$$\mathcal{F}_i = - \sum_{j \in \mathcal{S}} \rho Y_i D_{ij} (d_j + \chi_j (\ln T)'), \quad i \in \mathcal{S}, \quad (32)$$

$$q = \sum_{i \in \mathcal{S}} h_i \mathcal{F}_i + \sum_{j \in \mathcal{S}} \frac{RT}{m_j} \tilde{\chi}_j \mathcal{F}_j - \lambda T', \quad (33)$$

where $\tilde{\chi}_j$ is the rescaled thermal diffusion ratio of the j th species $\tilde{\chi}_j = \chi_j / X_j$. After some algebra, one establishes that the matrix \hat{L} is symmetric positive semi-definite with nullspace $N(\hat{L}) = \mathbb{R}u$ if and only if the matrix D is symmetric positive semi-definite with nullspace $N(D) = \mathbb{R}y$ and $\lambda > 0$.

Since the thermal diffusion coefficients $\theta = (\theta_1, \dots, \theta_{n^e})^t$ form a *vector* it is sufficient to introduce a *vector* of thermal diffusion ratios $\chi = (\chi_1, \dots, \chi_{n^e})^t$ in order to factorize the multicomponent diffusion matrix D with $\theta = D\chi$. Similarly, introducing the reduced thermal diffusion ratios $\hat{\chi}_j = RT\tilde{\chi}_j/m_j$, $j \in \mathcal{S}$, we may factorize the matrix \hat{L} in the coefficients $(\hat{L}_{1q}, \dots, \hat{L}_{n^e q})^t$ with $\hat{L}_{iq} = \sum_{j \in \mathcal{S}} \hat{L}_{ij} \hat{\chi}_j$, $i \in \mathcal{S}$. It is thus unnecessary to define *antisymmetric matrices* in order to factorize the matrices D , \hat{L} , or L in the vectors $(\theta_1, \dots, \theta_{n^e})^t$, $(\hat{L}_{1q}, \dots, \hat{L}_{n^e q})^t$, or $(L_{1q}, \dots, L_{n^e q})^t$, respectively. Such matrices α are indeed simply expressed as tensor products between the thermal diffusion ratios vector and the matrix nullspace vectors *and are even not unique* as soon as $n^e \geq 4$. Defining for instance $\hat{\alpha}_{ij} = \hat{\chi}_i - \hat{\chi}_j$, $i, j \in \mathcal{S}$, we have $\hat{L}_{iq} = \sum_{j \in \mathcal{S}} L_{ij} \hat{\alpha}_{ij}$, $i \in \mathcal{S}$, and $\hat{\alpha} = \hat{\chi} \otimes u - u \otimes \hat{\chi}$, where $u = (1, \dots, 1)^t$. Similarly, we have $L_{iq} = \sum_{j \in \mathcal{S}} L_{ij} (\hat{\chi}_j + h_j)$, and defining $\alpha_{ij} = \hat{\alpha}_{ij} + h_i - h_j$, $i, j \in \mathcal{S}$, we also have $L_{iq} = \sum_{j \in \mathcal{S}} L_{ij} \alpha_{ij}$, $i \in \mathcal{S}$.

To the authors' knowledge, the expressions (20)(21) associated with nonideal gas mixtures—taking into account the symmetry of the transport matrix—have first been written in the framework of thermodynamics of irreversible processes by Meixner [15, 16] and later by Prigogine [17, 18]. Similar expressions had been written previously by Eckart [53] but only *for ideal gas mixtures and without symmetry properties* of the transport coefficients. The expressions (20)(21) have then been rederived in various frameworks, in particular by Bearman and Kirkwood [20] (only partially) and Mori [21] with statistical mechanics, by Keizer [22] in the framework of statistical thermodynamics, and by Van Beijeren and Ernst [24] and Kurochkin et al. [25] in the

framework of the kinetic theory of dense gases, thanks to a modified form of Enskog equation [23]. The importance of Keizer’s results in statistical thermodynamics for high pressure combustion modeling has been emphasized in particular by Bellan, Harstad and coworkers [54, 11].

From a terminology point of view, the transport fluxes \mathcal{F}_i , $i \in \mathcal{S}$, q , and $q - \sum_{i \in \mathcal{S}} h_i \mathcal{F}_i$, are usually termed the species diffusion fluxes, the heat flux, and the reduced heat flux, respectively. In their remarkable paper on statistical mechanics, Irving and Kirkwood [19] have expressed the heat flux in terms of averages over molecular distribution functions and the corresponding expression has been termed the ‘Irving Kirkwood’ expression by Sarman and Evans [55]. This expression, however, is not a phenomenological relation expressing the heat flux in terms of macroscopic variable gradients and moreover does not concern mixtures [19]. It is thus inappropriate to term the heat flux or expression (21) the ‘Irving Kirkwood’ form of the heat flux. For a similar reason, it is inappropriate to term either the reduced heat flux or expression (26) the ‘Bearman Kirkwood’ form of the heat flux. Only the expressions of these fluxes *in the framework of statistical mechanics* and in terms of averages over molecular distributions should be termed the ‘Irving-Kirkwood’ and ‘Bearman-Kirkwood’ forms of the heat flux as originally meant by Sarman and Evans [55].

2.5 Entropy production

In order to assess the mathematical quality of the theoretical model presented in the previous sections, we have to establish that entropy production is nonnegative. The concavity properties of entropy—resulting from the construction of thermodynamics from the pressure law—will be discussed in Section 5.1. We only consider here the case of planar flame equations since it contains the main ingredients and since multidimensional problems are out of the scope of the present paper.

Introducing the entropy per unit mass of the mixture s , it is easily deduced from Gibbs relation that

$$Tds = -vdp - \sum_{k \in \mathcal{S}} g_k dY_k + dh,$$

where d denotes the total differential operator. Thanks to the isobaric flame equations we obtain $Tm s' = \sum_{i \in \mathcal{S}} g_i \mathcal{F}_i' - \sum_{i \in \mathcal{S}} g_i m_i \omega_i - q'$ so that the entropy governing equations reads

$$ms' + \left(- \sum_{i \in \mathcal{S}} \frac{g_i}{T} \mathcal{F}_i + \frac{q}{T} \right)' = - \sum_{i \in \mathcal{S}} \left(\frac{g_i}{T} \right)' \mathcal{F}_i + \left(\frac{1}{T} \right)' q - \sum_{i \in \mathcal{S}} \frac{g_i m_i \omega_i}{T}.$$

Entropy production associated with macroscopic gradients \mathbf{v}_L may thus be written

$$\mathbf{v}_L = - \sum_{i \in \mathcal{S}} \left(\frac{g_i}{T} \right)' \mathcal{F}_i + \left(\frac{1}{T} \right)' q = \langle Lw', w' \rangle, \quad (34)$$

where w is the variable $w = \left(-\frac{g_1}{T}, \dots, -\frac{g_{n^e}}{T}, \frac{1}{T} \right)^t$, w' its derivative, and the bracket $\langle \cdot, \cdot \rangle$ denotes the Euclidean scalar product. Since the matrix L is positive semi-definite, we conclude that entropy production associated with macroscopic gradients \mathbf{v}_L is nonnegative. Incidentally w is essentially the entropic variable [30] associated with the system of differential equations (1)(2).

In addition, \mathbf{v}_L is zero only when all gradients vanish, assuming that the mass fractions sum up to unity $\langle \mathbf{y}, \mathbf{u} \rangle = 1$ and that we are in the thermodynamic stability domain where the Hessian matrix $\partial_{\xi\xi}^2 s$ with respect to the thermodynamic variable $\xi = (v, Y_1, \dots, Y_{n^e}, e)^t$ is negative semi-definite with nullspace $N(\partial_{\xi\xi}^2 s) = \mathbb{R}\xi$. Denoting $\zeta = \left(\frac{p}{T}, -\frac{g_1}{T}, \dots, -\frac{g_{n^e}}{T}, \frac{1}{T} \right)^t$ we first note that $\zeta' = (\partial_{\xi\xi}^2 s)\xi'$ from Gibbs relation. Assuming that \mathbf{v}_L is zero, we then deduce from $N(L) = \mathbb{R}\mathcal{U}$ that $w' = \alpha\mathcal{U}$ with $\alpha \in \mathbb{R}$, so that $T' = 0$ since the last component of \mathcal{U} is zero, and next that $\langle \zeta', \xi' \rangle = 0$ using $T' = 0$, $p' = 0$ thanks to the isobaric framework, and $\langle \mathbf{y}', \mathbf{u} \rangle = 0$. Then from $\langle \xi', \zeta' \rangle = 0$ and $\zeta' = (\partial_{\xi\xi}^2 s)\xi'$ we obtain that $\langle \xi', (\partial_{\xi\xi}^2 s)\xi' \rangle = 0$ so that $\xi' \in \mathbb{R}\xi$ and $\xi' = 0$ since $\langle \mathbf{y}', \mathbf{u} \rangle = 0$ and all gradients vanish.

On the other hand, entropy production associated with chemistry \mathbf{v}_ω can be written

$$\mathbf{v}_\omega = - \sum_{i \in \mathcal{S}} \frac{g_i m_i \omega_i}{T} = -R \sum_{i \in \mathcal{S}} \mu_i \omega_i = -R \langle \mu, \omega \rangle, \quad (35)$$

where $\mu = (\mu_1, \dots, \mu_{n^e})^t$ and $\omega = (\omega_1, \dots, \omega_{n^e})^t$. Using then the vector relations $\omega = \sum_{j \in \mathcal{R}} (\nu_j^b - \nu_j^f) \tau_j$ where $\nu_j^b = (\nu_{1j}^b, \dots, \nu_{n^e j}^b)^t$ and $\nu_j^f = (\nu_{1j}^f, \dots, \nu_{n^e j}^f)^t$, for $j \in \mathcal{R}$, we obtain that $\mathbf{v}_\omega = -R \sum_{j \in \mathcal{R}} \langle \mu, \nu_j^b - \nu_j^f \rangle \tau_j$. However, we also have $\tau_j = \kappa_j^s (\exp \langle \nu_j^f, \mu \rangle - \exp \langle \nu_j^b, \mu \rangle)$, $j \in \mathcal{R}$, so that

$$\mathbf{v}_\omega = R \sum_{j \in \mathcal{R}} \kappa_j^s (\langle \nu_j^f, \mu \rangle - \langle \nu_j^b, \mu \rangle) (\exp \langle \nu_j^f, \mu \rangle - \exp \langle \nu_j^b, \mu \rangle). \quad (36)$$

Therefore, entropy production due to chemical reactions \mathbf{v}_ω is a sum of terms in the form $\alpha(x - y)(e^x - e^y)$ where α is positive so that \mathbf{v}_ω is nonnegative and only vanishes at chemical equilibrium, i.e., when $\langle \nu_j^f, \mu \rangle = \langle \nu_j^b, \mu \rangle$, $j \in \mathcal{R}$ [30, 49].

3 Thermochemistry and transport coefficients

We discuss in this section various coefficients associated with the theoretical model presented in Section 2.

3.1 Thermodynamics coefficients

The pure species attractive and repulsive massic parameters a_i and b_i , $i \in \mathcal{S}$, associated with the equation of state (7) may first be obtained from the species critical points. More specifically, assuming that the i th species is chemically stable, the attractive and repulsive parameters may be evaluated in the form [28]

$$a_i(T_{c,i}) = 0.42748 \frac{R^2 T_{c,i}^2}{m_i^2 p_{c,i}}, \quad b_i = 0.08664 \frac{RT_{c,i}}{m_i p_{c,i}}, \quad (37)$$

where $T_{c,i}$ and $p_{c,i}$ denote the corresponding critical temperature and pressure, respectively. A pure component fluid with the equation of state (7) and parameters (37) indeed displays a critical point located at temperature $T_{c,i}$ and pressure $p_{c,i}$. All the attractive and repulsive parameters of chemically stable species like H_2 , O_2 , N_2 or H_2O , may thus be determined from critical states conditions.

This procedure, however, cannot be generalized in a straightforward way to chemically unstable species like radicals since critical states *do not exist* for such species. More specifically, part of these molecules always recombine and prevent the existence of pure species states and the corresponding critical points. Moreover, combustion mixtures frequently contain such radicals or chemically unstable species. Arguing that these species are in small concentrations is neither satisfactory nor always true since—for instance—in the combustion products of a stoichiometric $\text{H}_2\text{-O}_2$ flame at 50 atm there are more than 18% of radicals like H, O, OH, or HO_2 .

However, the only physical quantities experienced by molecules during collisions are interaction potentials. One may thus wonder why state laws are not *solely* written in terms of interaction potentials parameters, eliminating any ambiguities with species critical states. Assuming that the i th species is a Lennard-Jones gas, for instance, it is possible to estimate [46, 47] the critical massic volume $v_{c,i}$ and the critical temperature $T_{c,i}$ from

$$v_{c,i} = (3.29 \pm 0.07) \frac{N \sigma_i^3}{m_i}, \quad T_{c,i} = (1.316 \pm 0.006) \frac{\epsilon_i}{k}, \quad (38)$$

where N is the Avogadro number, σ_i and ϵ_i the molecular diameter and Lennard-Jones potential well depth of the i th species, respectively. In term of attractive and repulsive parameters, this leads to the following expressions

$$a_i(T_{c,i}) = (5.55 \pm 0.12) \frac{N^2 \epsilon_i \sigma_i^3}{m_i^2}, \quad b_i = (0.855 \pm 0.018) \frac{N \sigma_i^3}{m_i}. \quad (39)$$

One could thus completely eliminate critical states data from an equation of state and use only molecular potential parameters as exemplified by Saur [6]. This procedure certainly clarifies the use of cubic equations of states for general mixtures involving radicals and in particular for combustion applications. More fundamentally, the success of the principle of corresponding states is closely associated with the existence of interaction potentials in the form $\epsilon\phi(r/\sigma)$ where σ is a characteristic length and ϵ a characteristic energy as discussed by Beattie [27] and Hirschfelder, Curtiss, and Bird [56].

Nevertheless, such a procedure—although theoretically satisfactory—is not accurate enough since chemically stable species do not exactly behave as Lennard-Jones gases or Stockmayer gases for polar molecules. Introducing the stable species critical states may thus be seen as a way of correcting interaction potential parameters taking into account a more complex behavior than that of Lennard-Jones. But we may still use the definitions associated with Lennard-Jones potentials for chemically unstable species and define for convenience a corresponding pseudo-critical state as given by (38). The relations (37) may thus finally be used for chemically stable species and the relations (39) for chemically unstable species like radicals with usual values for the Lennard-Jones parameters.

Once the attractive parameter $a_i(T_{c,i})$ at temperature $T_{c,i}$ is evaluated, its temperature dependence $a_i(T)$ is evaluated following Soave [41]

$$a_i(T) = a_i(T_{c,i})\alpha_i(T_i^*), \quad (40)$$

where $T_i^* = T/T_{c,i}$ is the i th species reduced temperature and α_i a nonnegative function of T_i^* . From physical considerations the coefficient α_i should be a decreasing function of the reduced temperatures T_i^* as pointed out by Ozokwelu and Erbar [57] and Grabovski and Daubert [58]. Since the coefficient α_i introduced by Soave does not satisfy such a property, it is first possible to truncate its temperature dependence in the form

$$\sqrt{\alpha_i} = \begin{cases} 1 + s_i(1 - \sqrt{T_i^*}), & \text{if } T_i^* \leq (1 + \frac{1}{s_i})^2, \\ 0, & \text{if } T_i^* \geq (1 + \frac{1}{s_i})^2, \end{cases} \quad (41)$$

where the quantity s_i depends on the i th species acentric factor ϖ_i [48]

$$s_i = 0.48508 + 1.5517\varpi_i - 0.151613\varpi_i^2. \quad (42)$$

These truncated coefficients $\sqrt{\alpha_i}$, $i \in \mathcal{S}$, and the original coefficients introduced by Soave $\sqrt{\alpha_i} = |1 + s_i(1 - \sqrt{T_i^*})|$, $i \in \mathcal{S}$, yield results that are in very close agreement since the crossing temperatures $T_{c,i}(1 + 1/s_i)^2$, $i \in \mathcal{S}$, are generally above 1000 K. At these temperatures, the specific volume is indeed already large and nonidealities then play a minor rôle.

A disadvantage of Soave corrective factors or their truncated version (41) is that they are not smooth with respect to temperature. In particular, for mixture of gases, they introduce small jumps in the temperature derivative of the attractive factor $\sqrt{a_i}$ and thereby of the attractive parameter $a = \sum_{i,j \in \mathcal{S}} Y_i Y_j \sqrt{a_i a_j}$ at the crossing temperatures $T_{c,i}(1 + 1/s_i)^2$, $i \in \mathcal{S}$. Even though such small jumps only arise in regions where the temperature is high and where nonidealities are negligible, it is sometimes preferable—at least from a numerical point of view—to have smooth attractive factors. Numerical spurious behavior has indeed been observed due to these small

discontinuities of the attractive factor temperature derivative. To this aim, we have preferred to use the new simple correlation

$$\sqrt{\alpha_i} = \begin{cases} 1 + s_i(1 - \sqrt{T_i^*}), & \text{if } T_i^* \leq 1, \\ 1 + \tanh(s_i(1 - \sqrt{T_i^*})), & \text{if } T_i^* \geq 1. \end{cases} \quad (43)$$

The left and right first and second derivatives of $\sqrt{\alpha_i}$ in (43) are identical for $T_i^* = 1$ so that the coefficient $\sqrt{\alpha_i}$ resulting from (43) is smoother than that of Soave $\sqrt{\alpha_i} = |1 + s_i(1 - \sqrt{T_i^*})|$ or truncated Soave (41). All these coefficients yield thermodynamic properties that are in very close agreement. Note that other exponential correlations have already been proposed in the literature but involving the square root of the acentric factor [57] which is negative for species like hydrogen.

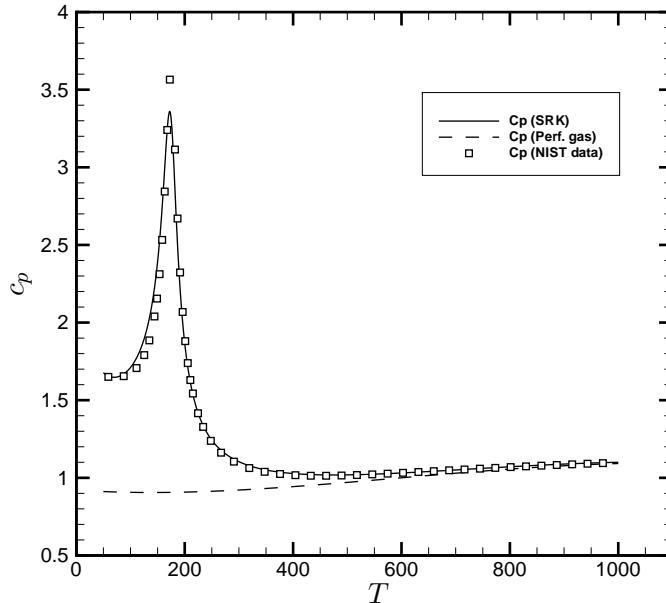


Figure 1: Specific heat at constant pressure c_p of the O_2 species at $p = 100$ atm

The thermodynamic properties of perfect gases have finally been evaluated from the NIST/JANAF Thermochemical Tables as well as from the NASA coefficients [59, 60]. As a typical illustration, we present in Figure 1 the constant pressure specific heat c_p of the species O_2 evaluated from the Soave-Redlich-Kwong equation of state as well as NIST Standard Reference Data for comparison. This figure shows that the SRK equation of state and the associated thermochemistry parameters yield very good predictions unlike the perfect gas model which is not accurate at low temperatures.

3.2 Chemical kinetic coefficients

The symmetric reaction constant κ_j^s of the j th reaction may be determined from the forward reaction constant κ_j^f thanks to (18) as discussed in Section 2.3. From a practical point of view, however, it is somewhat more convenient to use the classical formalism (15) and to replace the perfect gas molar concentrations γ_i^{PG} , $i \in \mathcal{S}$, by the activities $a_i = \exp(\mu_i - \mu_i^{\text{u,PG}})$, $i \in \mathcal{S}$, respectively.

We have used a reaction mechanism mainly due to Warnatz [61] with forward rates in Arrhenius form $\kappa_j^f(T) = \mathfrak{A}_j T^{\mathfrak{b}_j} \exp(-\mathfrak{E}_j/RT)$, $j \in \mathcal{R}$, and with kinetic parameters \mathfrak{A}_j , \mathfrak{b}_j and \mathfrak{E}_j ,

$j \in \mathcal{R}$, as in Table 1.

Table 1: Warnatz kinetics scheme for hydrogen combustion [61]

i	Reaction	\mathfrak{A}_i	\mathfrak{b}_i	\mathfrak{C}_i
1	$\text{H} + \text{O}_2 \rightleftharpoons \text{OH} + \text{O}$	2.00E+14	0.00	16802.
2	$\text{O} + \text{H}_2 \rightleftharpoons \text{OH} + \text{H}$	5.06E+04	2.67	6286.
3	$\text{OH} + \text{H}_2 \rightleftharpoons \text{H}_2\text{O} + \text{H}$	1.00E+08	1.60	3298.
4	$2\text{OH} \rightleftharpoons \text{O} + \text{H}_2\text{O}$	1.50E+09	1.14	100.
5	$\text{H} + \text{H} + \text{M} \rightleftharpoons \text{H}_2 + \text{M}^a$	6.30E+17	-1.00	0.
6	$\text{H} + \text{OH} + \text{M} \rightleftharpoons \text{H}_2\text{O} + \text{M}^a$	7.70E+21	-2.00	0.
7	$\text{O} + \text{O} + \text{M} \rightleftharpoons \text{O}_2 + \text{M}^a$	1.00E+17	-1.00	0.
8	$\text{H} + \text{O}_2 + \text{M} \rightleftharpoons \text{HO}_2 + \text{M}^a$	8.05E+17	-0.80	0.
9	$\text{H} + \text{HO}_2 \rightleftharpoons 2\text{OH}$	1.50E+14	0.00	1004.
10	$\text{H} + \text{HO}_2 \rightleftharpoons \text{H}_2 + \text{O}_2$	2.50E+13	0.00	693.
11	$\text{H} + \text{HO}_2 \rightleftharpoons \text{H}_2\text{O} + \text{O}$	3.00E+13	0.00	1721.
12	$\text{O} + \text{HO}_2 \rightleftharpoons \text{O}_2 + \text{OH}$	1.80E+13	0.00	-406.
13	$\text{OH} + \text{HO}_2 \rightleftharpoons \text{H}_2\text{O} + \text{O}_2$	6.00E+13	0.00	0.
14	$\text{HO}_2 + \text{HO}_2 \rightleftharpoons \text{H}_2\text{O}_2 + \text{O}_2$	2.50E+11	0.00	-1242.
15	$\text{OH} + \text{OH} + \text{M} \rightleftharpoons \text{H}_2\text{O}_2 + \text{M}^a$	1.14E+22	-2.00	0.
16	$\text{H}_2\text{O}_2 + \text{H} \rightleftharpoons \text{HO}_2 + \text{H}_2$	1.70E+12	0.00	3752.
17	$\text{H}_2\text{O}_2 + \text{H} \rightleftharpoons \text{H}_2\text{O} + \text{OH}$	1.00E+13	0.00	3585.
18	$\text{H}_2\text{O}_2 + \text{O} \rightleftharpoons \text{HO}_2 + \text{OH}$	2.80E+13	0.00	6405.
19	$\text{H}_2\text{O}_2 + \text{OH} \rightleftharpoons \text{H}_2\text{O} + \text{HO}_2$	5.40E+12	0.00	1004.

^a third body efficiency $\text{H}_2 = 2.86$, $\text{N}_2 = 1.43$, $\text{H}_2\text{O} = 18.6$

Units are moles, centimeters, seconds, calories, and Kelvins

3.3 Transport coefficients

The species diffusion fluxes—or equivalently the species diffusion velocities—are evaluated by using Stefan-Maxwell equations derived from the kinetic theory of dense gases by Kurochkin, Makarenko, and Tirsikii [25] as well as from various experiments with liquid mixtures as comprehensively discussed by Taylor and Krishna [31]. Another variant is to use Grad’s moments method as done by Harstad and Bellan [54]. Grad’s moments method, however, has been shown to be equivalent to the Chapman-Enskog method by Zhdanov in the framework of weakly ionized plasmas [62]. In particular, Harstad and Bellan have also obtained Stefan-Maxwell type equations for high pressure diffusion coefficients [54]. On the other hand, even though the thermodynamics of irreversible processes yields the structure of transport fluxes, it *cannot* provide the corresponding transport coefficients.

The Stefan-Maxwell equations associated with first order diffusion coefficients are the n^e linear systems of size n^e in the form [65, 25]

$$\begin{cases} \Delta \mathbf{a}^k = \mathbf{b}^k, \\ \langle \mathbf{a}^k, \mathbf{y} \rangle = 0, \end{cases} \quad k \in \mathcal{S}, \quad (44)$$

where $\Delta \in \mathbb{R}^{n^e, n^e}$ is the Stefan-Maxwell matrix, $\mathbf{b}^k, \mathbf{y} \in \mathbb{R}^{n^e}$, $k \in \mathcal{S}$, are given vectors, $\mathbf{a}^k \in \mathbb{R}^{n^e}$, $k \in \mathcal{S}$, are the unknown vector, and $\langle \cdot, \cdot \rangle$ denotes the Euclidean scalar product. The Stefan-Maxwell matrix Δ is given by [25, 64, 65, 30, 54]

$$\Delta_{kk} = \sum_{\substack{l \in \mathcal{S} \\ l \neq k}} \frac{x_k x_l}{\mathcal{D}_{kl}}, \quad k \in \mathcal{S}, \quad \Delta_{kl} = -\frac{x_k x_l}{\mathcal{D}_{kl}}, \quad k, l \in \mathcal{S}, \quad k \neq l,$$

where x_1, \dots, x_{n^e} are the species mole fractions, \mathcal{D}_{kl} , $k, l \in \mathcal{S}$, the species binary diffusion coefficients, and $\mathbf{y} = (Y_1, \dots, Y_{n^e})^t$ is the mass fractions vector. The right hand sides \mathbf{b}^k , $k \in \mathcal{S}$,

are given by $\mathbf{b}^k = \mathbf{e}^k - \mathbf{y}$, $k \in \mathcal{S}$, where \mathbf{e}^k , $k \in \mathcal{S}$, are the standard basis vectors of \mathbb{R}^{n^e} or equivalently by $\mathbf{b}_i^k = \delta_{ki} - Y_i$, $i, k \in \mathcal{S}$, and we have assumed that the mass fractions sum up to unity $\langle \mathbf{y}, \mathbf{u} \rangle = 1$. The transport linear systems (44) are easily shown to be well posed [65, 30] and the first order diffusion coefficients are evaluated from

$$D_{kl} = \langle \mathbf{a}^k, \mathbf{b}^l \rangle = \mathbf{a}_l^k = \mathbf{a}_k^l, \quad k, l \in \mathcal{S}. \quad (45)$$

The matrix D is positive semi-definite with nullspace $\mathbb{R}\mathbf{y}$ [64, 65, 30] and the numerical inversion of the Stefan-Maxwell equations is discussed in Section 4.1.

The diffusion velocities, defined by $\mathcal{F}_i = \rho Y_i U_i$, are then given by

$$U_i = - \sum_{j \in \mathcal{S}} D_{ij} (d_j + \chi_j T'/T), \quad i \in \mathcal{S}, \quad (46)$$

where $\chi_1, \dots, \chi_{n^e}$ are the thermal diffusion ratios. By multiplying the k th linear system (44) by $d_k + \chi_k T'/T$ and by summing over k we also obtain the Stefan-Maxwell equations in vector form. More specifically, introducing the linearly constrained diffusion driving forces $\tilde{d}_i = d_i - Y_i \sum_{j \in \mathcal{S}} d_j$, $i \in \mathcal{S}$, the corresponding vector $\tilde{\mathbf{d}} = (\tilde{d}_1, \dots, \tilde{d}_{n^e})^t$, the diffusion velocities vector $\mathbf{U} = (U_1, \dots, U_{n^e})^t$, and the thermal diffusion ratios vector $\chi = (\chi_1, \dots, \chi_{n^e})^t$, the Stefan-Maxwell equations in vector form read [64, 31, 30, 78, 77]

$$\begin{cases} \Delta \mathbf{U} = -(\tilde{\mathbf{d}} + \chi T'/T), \\ \langle \mathbf{U}, \mathbf{y} \rangle = 0. \end{cases} \quad (47)$$

These equations are equivalent to the Stefan-Maxwell equations for the diffusion coefficients (44) upon giving all possible values to the driving forces d_1, \dots, d_{n^e} .

In order to evaluate the binary diffusion coefficients at high pressure \mathcal{D}_{ij} , $i, j \in \mathcal{S}$, we have used the kinetic theory of dense gas mixtures [25]. The corresponding binary diffusion coefficients are in the form

$$\mathcal{D}_{ij} = \frac{n^{\text{st}} \mathcal{D}_{ij}^{\text{st}}}{n} \frac{1}{\Upsilon_{ij}}, \quad (48)$$

where n denotes the molar concentration of the mixture, n^{st} the perfect gas concentration at the standard pressure p^{st} , $\mathcal{D}_{ij}^{\text{st}}$ the binary diffusion coefficient at the standard pressure p^{st} given by the kinetic theory of dilute gases [50, 52, 65, 30], and Υ_{ij} a statistical factor associated with the reduction of the free volume during collisions between molecules of the i th and j th species. Within the framework of the kinetic theory of dense gas mixtures the factor Υ_{ij} can be written [25]

$$\Upsilon_{ij} = 1 + \sum_{k \in \mathcal{S}} \frac{\pi \mathbf{n}_k}{12} \left(8(\sigma_{ik}^3 + \sigma_{jk}^3) - 6(\sigma_{ik}^2 + \sigma_{jk}^2) \sigma_{ij} - 3(\sigma_{ik}^2 - \sigma_{jk}^2)^2 \sigma_{ij}^{-1} + \sigma_{ij}^3 \right), \quad (49)$$

where \mathbf{n}_i denotes the density number of the i th species and σ_{ij} the collision diameter between the i th and j th species. For binary mixtures, that is, for $\mathcal{S} = \{i, j\}$, this factor Υ_{ij} reduces to the one given by the Enskog-Thorne theory.

The matrix Γ is given by $\Gamma_{jl} = x_j \partial_{x_i} \mu_j$, $j, l \in \mathcal{S}$, and we have the vector relation $\mathbf{d} = \Gamma \mathbf{x}'$ where $\mathbf{x}' = (x'_1, \dots, x'_{n^e})^t$ denotes the vector of mole fractions derivatives. As a consequence, we can write the diffusion velocities vector \mathbf{U} in the form

$$\mathbf{U} = -D(\Gamma \mathbf{x}' + \chi T'/T), \quad (50)$$

so that thermodynamic nonidealities are factorized through the matrix Γ even though high pressure effects are also taken into account in the multicomponent diffusion matrix D . This point is of fundamental importance since numerous experiments have established that the multicomponent diffusion coefficient matrix D is *much smoother and more convenient to evaluate* than the

combined matrix $D\Gamma$ as discussed by Hirschfelder, Curtiss, and Bird [56] and Taylor and Krishna [31].

Thermal diffusion effects are generally important in H_2 -Air and H_2 - O_2 flames [67, 68, 69]. On the one hand, the usual liquid part of the Soret coefficient for the j th species associated with the formulation (20)(21) simply corresponds to the derivative of $m_j g_j / T$ with respect to temperature at constant pressure and mass—or mole—fractions $\partial_T(m_j g_j / T) = -m_j h_j / T^2$ although it is often written in a confusing form [66]. On the other hand, using the formulation (25)(26) and in order to evaluate the thermal diffusion ratios χ_i , $i \in \mathcal{S}$, we have generally used the limiting dilute gas value for χ_i , $i \in \mathcal{S}$. The main idea is that thermal diffusion will mainly influence the part of the flame which is sufficiently warm. Note that high pressure effects are still taken into account in the corresponding thermal diffusion coefficients $\theta = D\chi$ through the matrix D which involves high pressure diffusion coefficients. A high pressure correction—of thermodynamic origin—for the thermal diffusion ratios has also been suggested by Kurochkin, Makarenko, and Tirsikii [25]. This correction, however, seems to be incompatible with the thermodynamics of irreversible processes, since the derivative of the reduced potential $m_j g_j / T$ *strictly* yields the enthalpy term $-m_j h_j / T^2$.

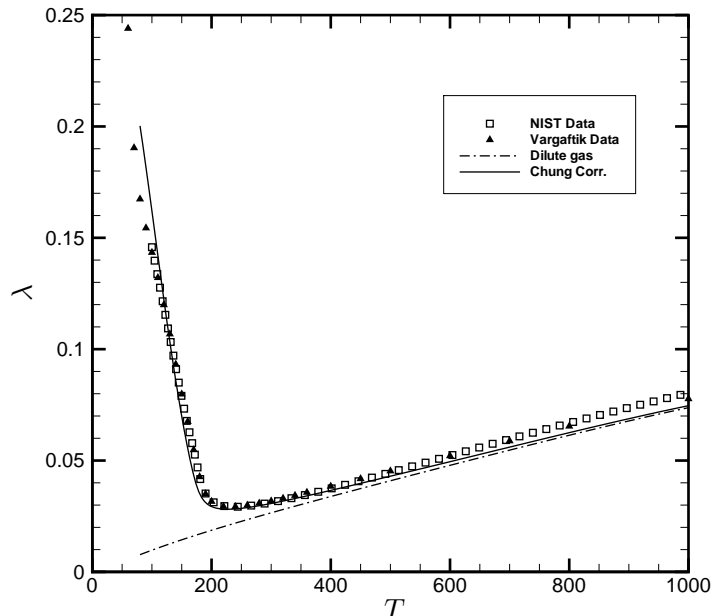


Figure 2: Thermal conductivity λ of the O_2 species at $p = 100$ atm

The thermal conductivity has been evaluated from the correlation proposed by Chung et al. [70] and the correlation proposed by Ely and Hanley [71] yields similar results. Chung et al. have written the thermal conductivity as the sum of a dilute-gas conductivity λ^{dil} corrected by a density dependent factor β and a specific high-density thermal conductivity λ^{hp}

$$\lambda = \lambda^{\text{dil}}\beta + \lambda^{\text{hp}}. \quad (51)$$

Detailed expressions for β and λ^{hp} can be found in [70] and are presented in Appendix B. The thermal conductivity of dilute mixtures λ^{dil} has been evaluated by solving the corresponding transport linear system obtained from the kinetic theory of dilute gases [65, 72, 67]. As a typical illustration, we present in Figure 2 the thermal conductivity λ of the species O_2 obtained from (51) as a function of temperature T together with experimental data from NIST/Laesecke et al. [73] and Vargaftik et al. [74], as well as the thermal conductivity λ^{dil} of dilute gases which is not accurate for low temperatures.

4 Computational considerations

We discuss here numerical details which are important for a successful implementation of the high pressure flame model presented in the previous sections and we discuss various test cases for the chemical source terms investigated in Section 6.1.

4.1 Diffusion matrices

Evaluating diffusion coefficients by solving the n^e Stefan-Maxwell transport linear systems (44) is generally required when an implicit time marching technique is used to solve the flame equations. On the contrary, when an explicit time technique is used, it is sufficient to solely evaluate the diffusion velocities by solving the Stefan-Maxwell equations in vector form (47).

The Stefan-Maxwell matrix Δ is symmetric positive semi-definite with nullspace $N(\Delta) = \mathbb{R}\mathbf{u}$ where $\mathbf{u} = (1, \dots, 1)^t \in \mathbb{R}^{n^e}$ and $2\text{diag}(\Delta) - \Delta$ is positive definite when $n^e \geq 3$ [64, 30, 75]. Defining $Q = \mathbb{I}_{n^e} - \mathbf{y} \otimes \mathbf{u} = [\mathbf{b}^1, \dots, \mathbf{b}^{n^e}]$, the transport linear systems (44) can be rewritten in the matrix form

$$\Delta D = Q,$$

and we also have $D\mathbf{y} = 0$ where it has been assumed that $\langle \mathbf{y}, \mathbf{u} \rangle = 1$. One can establish that D is the generalized inverse of Δ with prescribed nullspace $\mathbb{R}\mathbf{y}$ and range \mathbf{y}^\perp and that for any $\alpha > 0$ we have $D = (\Delta + \alpha \mathbf{y} \otimes \mathbf{y})^{-1} - (1/\alpha)\mathbf{u} \otimes \mathbf{u}$ [64, 65, 75, 30].

As a direct application of the theory of iterative algorithms for singular systems [64, 65, 75, 30] we deduce that, using the splitting $\Delta = M - W$ where

$$M = \text{diag}\left(\frac{\Delta_{11}}{1 - Y_1}, \dots, \frac{\Delta_{n^e n^e}}{1 - Y_{n^e}}\right), \quad (52)$$

and letting $\mathcal{T} = M^{-1}W$ and $P = Q^t = \mathbb{I}_{n^e} - \mathbf{u} \otimes \mathbf{y}$, we have the convergent asymptotic expansion [64, 65, 75, 30]

$$D = \sum_{0 \leq j < \infty} (P\mathcal{T})^j P M^{-1} P^t. \quad (53)$$

Considering the first term $P M^{-1} P^t$, the matrix M^{-1} corresponds to a generalization to high pressure of the Hirschfelder-Curtiss approximation and the projector P to the addition of a species independent mass conservation corrector [64, 78]. The next approximation of D with two terms is more interesting since it is much more accurate and still yields $(n^e)^2$ coefficients within $\mathcal{O}((n^e)^2)$ operations [67, 64, 75]. Harstad and Bellan have checked in particular that this two term approximation is accurate for high pressures [54]. Even the highly accurate three term approximation is interesting from a computational point of view since—thanks to symmetry—it is still approximately half the cost of a direct method using Cholesky algorithm with n^e backsolves. These iterative algorithms have generally been found to be very effective for fast and accurate evaluation of multicomponent diffusion matrices [64, 75, 76, 77].

4.2 Nonidealities in diffusion fluxes

From the expression of diffusion velocities $U = -D(\Gamma X' + \chi T'/T)$ one may first think that it is necessary to evaluate the matrix Γ associated with nonidealities and next to perform the matrix product $D\Gamma$ in order to evaluate the species diffusion velocities U . Such a procedure, however, would be costly and turns out to be unnecessary.

Indeed, the diffusion driving force d_i of the i th species is given by $d_i = x_i(\mu_i)'_T$ where $'_T$ denotes the derivative operator at fixed temperature in the variables $(p, x_1, \dots, x_{n^e}, T)$ or equivalently $(p, Y_1, \dots, Y_{n^e}, T)$. We may thus directly evaluate the derivatives $(\mu_i)'_T$, $i \in \mathcal{S}$, and then the diffusion velocities, thereby avoiding both the evaluation of the matrix Γ and the matrix product $D\Gamma$. The derivatives at constant temperature are easily evaluated whatever the discretization method, finite differences, finite elements, or finite volumes. For finite differences, for instance,

and in a one dimensional isobaric context associated with planar flames, the derivative $(\mu_i)'_{T,k+\frac{1}{2}}$ at the grid midpoint $x_{k+\frac{1}{2}} = \frac{1}{2}(x_k + x_{k+1})$ is simply evaluated in the form

$$(\mu_i)'_{T,k+\frac{1}{2}} = \frac{\mu_i(p, Y_{1,k+1}, \dots, Y_{n^e,k+1}, T_{k+\frac{1}{2}}) - \mu_i(p, Y_{1,k}, \dots, Y_{n^e,k}, T_{k+\frac{1}{2}})}{x_{k+1} - x_k},$$

where $T_{k+\frac{1}{2}}$ denotes the temperature at the grid midpoint $x_{k+\frac{1}{2}}$, p the constant pressure, and $Y_{i,k}$ the mass fraction of the i th species at the k th grid point.

One more precaution is actually necessary since the potential μ_i is singular when the molar fraction of the i th species goes to zero. However, this potential μ_i may be decomposed in the form

$$\mu_i = \ln X_i + \mu_i^{\text{sm}}, \quad (54)$$

where the smooth part $\mu_i^{\text{sm}} = \mu_i^{\text{u}} - \ln(mv)$ is given by

$$\begin{aligned} \mu_i^{\text{sm}} = & \frac{m_i g_i^{\text{PG}^*}}{RT} + \ln\left(\frac{RT}{(v-b)p^{\text{st}}m}\right) + \sum_{j \in \mathcal{S}} \frac{Y_j}{m_j} \frac{m_i b_i}{v-b} - \frac{m_i a b_i}{RT b(v+b)} \\ & + \frac{a b_i - b \partial_{Y_i} a}{b^2} \frac{m_i}{RT} \ln\left(1 + \frac{b}{v}\right), \end{aligned} \quad (55)$$

where $g_i^{\text{PG}^*}$ denotes the perfect gas Gibbs function of the i th species at pressure p^{st} , so that d_i may be evaluated as $d_i = X_i' + X_i(\mu_i^{\text{sm}})'_T$. A similar procedure may also be used with the formulation (20)(21) involving the full derivatives μ_i' , $i \in \mathcal{S}$, of the potentials μ_i , $i \in \mathcal{S}$. We have preferred to use (25)(26) in order to accurately evaluate the species enthalpies h_j , $j \in \mathcal{S}$, appearing in the transport fluxes.

4.3 Continuation methods

The flame governing equations are discretized by using finite differences and solved by using Newton's method and self adaptive grids [79]. Pseudo unsteady iterations are used to bring the initial guess into the domain of convergence of steady Newton's iterations [79]. We typically use one thousand grid points with the flame front located at $x^{\text{fx}} = 1$ with $T^{\text{fx}} = 500$ K.

Once a first flame structure is obtained, continuation techniques are used to generate solution branches depending on a parameter like the equivalence ratio φ or the fresh gas temperature T^{fr} . These techniques involve reparameterization of solution branches and global static rezone adaptive gridding [80]. The quantity used to reparameterize solution branches corresponds to the solution component whose tangent derivative is the largest in absolute value [80]. This method is optimal and *automatically* selects the best component to be used for reparameterization [80], such as the temperature in a moving flame front. In comparison, techniques using an a priori selected fixed solution component are suboptimal implementations of continuation algorithms.

Highly optimized thermochemistry and transport routines have been extended to the high pressure domain and have been used in order to evaluate chemical production rates, thermodynamic properties and transport coefficients [81, 82, 76].

Similar continuation techniques have also been used to investigate the location of nontrivial zero eigenvalues of entropy Hessian matrices in order to determine the thermodynamic stability domains of fresh mixtures as discussed in Section 5.

4.4 Chemistry test cases

In order to evaluate the influence of reaction rates nonidealities on laminar flame structures, four different chemistry models have been investigated.

The first model—referred to as PG—uses the perfect gas formulation (15) with the species molar concentration evaluated as for perfect gases

$$\gamma_j^{\text{PG}} = \frac{X_j p}{RT}, \quad j \in \mathcal{S}. \quad (56)$$

In this model, the forward reaction constant is in standard Arrhenius form and the equilibrium constant is given by (16).

The second model—referred to as PG-HP—uses the the perfect gas formulation (15) but with concentrations evaluated from the high pressure massic volume v

$$\gamma_j = \frac{Y_j}{m_j v}. \quad (57)$$

The equilibrium displacement is then a consequence of the Le Chatellier’s principle.

The third model—referred to as Hybrid—is an inconsistent attempt to take into account real-gas effects in chemical source terms. The real-gas predicted molar concentrations (57) are used and the equilibrium constant takes into account nonidealities in the form

$$\kappa_j^{\text{eq}} = \exp\left(\sum_{l \in \mathcal{S}} (\nu_{lj}^f - \nu_{lj}^b) \mu_l^u\right), \quad j \in \mathcal{R}. \quad (58)$$

In other words, the concentrations γ_j , $j \in \mathcal{S}$, are used in the forward rates whereas the activities a_j , $j \in \mathcal{S}$, are used in the equilibrium constants, so that this often used model is *inconsistent*. In addition, the forward and reverse reactions do not play a symmetric rôle.

The last model—referred to as Nonideal—is the rate of progress given by statistical thermodynamics (14). This formulation is equivalent to using the classical reaction rates formulation (15) with the molar concentration γ_j replaced by the activities

$$a_j = \exp(\mu_j - \mu_j^{\text{u,PG}}). \quad (59)$$

In contrast with the hybrid model, the activities now are used in both the forward rates and the equilibrium constants—and therefore also in the reverse rates. Finally, this model is the only one consistent with nonideal thermodynamics, i.e., the only model which insures positivity of entropy production.

5 Thermodynamic stability of premixed states

We discuss in this section the thermodynamic stability of mixture states. Thermodynamic stability of fresh premixed reactants is naturally of fundamental importance for planar transcritical flames.

5.1 Entropy concavity

From the second principle of thermodynamics, the evolution of an isolated system tends to maximize its entropy. The entropy of a stable isolated homogeneous system should thus be a concave function of its volume, composition variables, and internal energy. Whenever it is not the case, the system loses its homogeneity and splits between two or more phases in order to reach equilibrium.

Denoting by $\xi = (v, Y_1, \dots, Y_{n^e}, e)^t$ the thermodynamic variable, the Hessian matrix $\partial_{\xi\xi}^2 s$ must therefore be negative semi-definite with nullspace $N(\partial_{\xi\xi}^2 s) = \mathbb{R}\xi$. The thermodynamic variable ξ is always in the nullspace of the Hessian matrix thanks to homogeneity properties of Gibbsian type thermochemistry [30]. The semi-definite negativity of the entropy hessian $\partial_{\xi\xi}^2 s$ has been checked by investigating its eigenvalues.

Let us denote by ϕ the difference between the pressure p and the perfect gas pressure p^{PG} obtained for the same ξ so that

$$p = p^{\text{PG}} + \phi. \quad (60)$$

Let also denote by $\tilde{\partial}$ the derivative operator with respect to the natural variable $\psi = (v, Y_1, \dots, Y_{n^e}, T)^t$ and by $f^v, f^1, \dots, f^{n^e}, f^e$ the canonical basis of \mathbb{R}^{n^e+2} . After lengthy calculations, the Hessian ma-

trix $\partial_{\xi\xi}^2 s$ with respect to the thermodynamic variable ξ can be written in the form

$$\begin{aligned} \partial_{\xi\xi}^2 s &= \frac{\tilde{\partial}_v \phi}{T} \mathbf{f}^v \otimes \mathbf{f}^v + \sum_{i \in \mathcal{S}} \frac{\tilde{\partial}_{Y_i} \phi}{T} (\mathbf{f}^v \otimes \mathbf{f}^i + \mathbf{f}^i \otimes \mathbf{f}^v) - \sum_{i \in \mathcal{S}} \frac{R Y_i}{v^2 m_i} (\mathbf{f}^v - \frac{v}{Y_i} \mathbf{f}^i) \otimes (\mathbf{f}^v - \frac{v}{Y_i} \mathbf{f}^i) \\ &\quad - \sum_{i,j \in \mathcal{S}} \frac{\mathbf{f}^i \otimes \mathbf{f}^j}{T} \int_v^\infty \tilde{\partial}_{Y_i Y_j}^2 \phi dv' - \frac{\mathbf{t} \otimes \mathbf{t}}{T^2 c_v}, \end{aligned} \quad (61)$$

where $\mathbf{t} = -\tilde{\partial}_v e \mathbf{f}^v - \sum_{i \in \mathcal{S}} \tilde{\partial}_{Y_i} e \mathbf{f}^i + \mathbf{f}^e$ and \otimes is the tensor product symbol. Moreover, we have $\langle \mathbf{t}, \xi \rangle = 0$, $(\partial_{\xi\xi}^2 s) \xi = 0$, and ξ can be written $\xi = v \mathbf{f}^v + \sum_{i \in \mathcal{S}} Y_i \mathbf{f}^i + e \mathbf{f}^e$.

After some linear algebra, thanks to $c_v > 0$, one can establish that $\partial_{\xi\xi}^2 s$ is negative semi-definite with nullspace $N(\partial_{\xi\xi}^2 s) = \mathbb{R} \xi$ if and only if the matrix Λ of size n^e defined by

$$\Lambda = \sum_{i \in \mathcal{S}} \frac{R}{m_i Y_i} \mathbf{e}^i \otimes \mathbf{e}^i + \sum_{i,j \in \mathcal{S}} \frac{\mathbf{e}^i \otimes \mathbf{e}^j}{T} \int_v^\infty \tilde{\partial}_{Y_i Y_j}^2 \phi dv', \quad (62)$$

is positive definite, where $\mathbf{e}^1, \dots, \mathbf{e}^{n^e}$ denotes the canonical basis of \mathbb{R}^{n^e} . The required thermal stability condition $c_v > 0$ is further guaranteed by the SRK equation of state as detailed in Appendix C.

The thermodynamic stability domain where the mixture is locally stable is thus the domain where the matrix Λ is positive definite. Moreover, the mixture is also globally stable on every convex set—with respect to the variable ξ —included in this stability domain. Several informations may be gained on this stability domain by inspecting various limiting cases. A first important situation is the low density limit $v \rightarrow \infty$. In this limit, the matrix Λ is effectively positive definite since it asymptotically reduces to the positive definite diagonal matrix

$$\lim_{v \rightarrow \infty} \Lambda = R \operatorname{diag} \left(\frac{1}{m_1 Y_1}, \dots, \frac{1}{m_{n^e} Y_{n^e}} \right).$$

A second interesting asymptotic limit is that of pure species states. Assuming for instance that asymptotically $\mathbf{y} = (Y_1, \dots, Y_{n^e})^t$ approaches the base vector \mathbf{e}^i , then the terms $R/m_j Y_j$ on the diagonal of Λ become dominant for $j \neq i$. In addition, the base vector \mathbf{e}^i is asymptotically the i th eigenvector and the identity

$$\sum_{i,j \in \mathcal{S}} Y_i Y_j \Lambda_{ij} = -\frac{v^2}{T} \partial_v p, \quad (63)$$

indicates that the i th eigenvalue is also positive as soon as $\partial_v p < 0$. This stability condition is guaranteed for all temperatures if the pressure p is above the critical pressure $p_{c,i}$ of the i th species.

5.2 Stability limit

The eigenvalue decomposition of the matrix Λ is a rather expensive operation. Thermodynamic stability of planar flames mixture states has thus been checked after the calculation of each flame structure. When nonidealities are *not* taken into account in diffusive processes, numerical experience shows that it is indeed possible to compute flames with thermodynamically unstable fresh mixtures associated with positive eigenvalues of the entropy Hessian matrix $\partial_{\xi\xi}^2 s$. On the contrary, when transport nonidealities are taken into account, whenever the fresh mixture is thermodynamically unstable, numerical methods generally diverge, the system of equations having lost its elliptic nature. In this situation, at the worst, a converged solution may eventually be at the onset of the instability domain.

Independently, an exhaustive study of the thermodynamic stability of ternary mixtures $\text{H}_2\text{-O}_2\text{-N}_2$ has been performed at pressure 100 atm. Similar results have also been obtained at

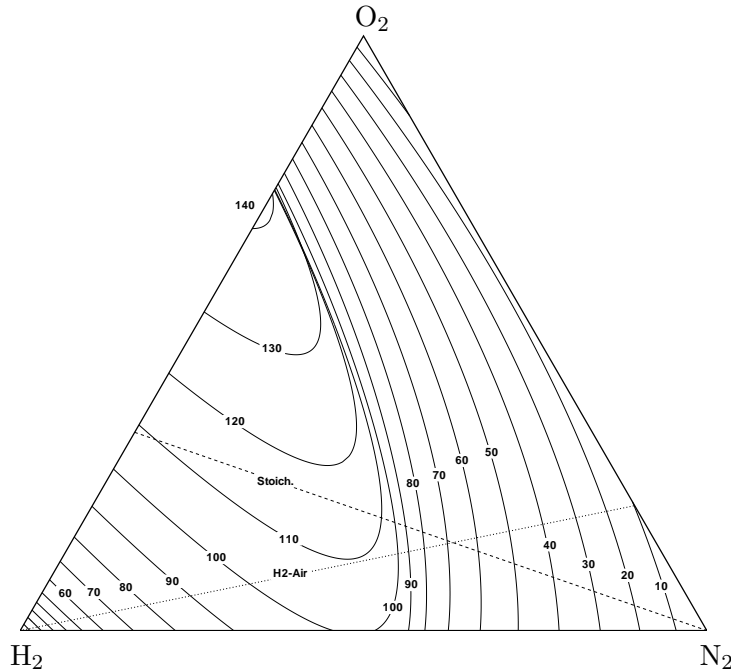


Figure 3: Thermodynamic stability limits isotherms for ternary $\text{H}_2\text{-O}_2\text{-N}_2$ mixture at 100 atm

different pressures as long as they are above the critical pressures of H_2 , O_2 , and N_2 . In order to investigate the corresponding stability domain, we have located the points where the first eigenvalue of the matrix Λ is changing of sign by inspecting the zero values of its determinant. To this aim, we have used continuation methods in order to generate the whole stability domain.

Note that the thermodynamic stability domain only depends on the equation of state. That is, it depends on the state of the mixture $T, v, Y_1, \dots, Y_{n^e}$, on the attractive and repulsive parameters a and b , and on R, m_1, \dots, m_{n^e} . In particular, this thermodynamic stability domain is independent of the perfect gas thermodynamic properties $c_{pi}^{\text{PG}}, e_i^{\text{PG}}$, and $s_i^{\text{PG}}, i \in \mathcal{S}$, and may be computed for all temperatures where a is defined. Of course, when the temperature is too low, the equation of state is not anymore valid, and the species may be in solid state, but we still performed the calculation to investigate the numerical behavior of the Hessian matrix.

The boundaries of the stability domain for various fixed temperatures and at $p = 100$ atm are presented in Figure 3. The lines correspond to the locus of the first zero of the determinant of Λ for various fixed temperatures. The stable zones are easily identified since they include the corners associated with pure species states. The unstable zone starts above 140 K between H_2 and O_2 , increases as T decreases, and reach the $\text{H}_2\text{-N}_2$ boundary around 100 K. The binary $\text{O}_2\text{-N}_2$ mixture is also predicted to be stable down to very low temperatures. The presence of H_2 thus has a destabilizing effect and rises the stability limit up to 140 K in $\text{H}_2\text{-O}_2$ binary mixtures and up to 100 K in $\text{H}_2\text{-N}_2$ binary mixtures.

Figures 4 and 5 give some views of the previous ternary diagram for specific mixtures such as binary, stoichiometric, $\text{H}_2\text{-Air}$, and $\text{H}_2\text{-O}_2$, mixtures.

The stability limits presented in Figure 3 should not be confused with *fixed composition* mechanical stability limits. More specifically, if we only require that the matrix Λ is positive definite along the vector $\mathbf{y} = (Y_1, \dots, Y_{n^e})^t$ then, from (63), we will solely require that $\partial_v p < 0$ which is precisely the fixed-composition mechanical equilibrium condition. The corresponding *fixed composition* stability limit is then such that $\partial_v p = 0$ and we investigated the *extreme* fixed composition mechanical stability limits for which we both have $\partial_v p = 0$ and $\partial_{vv}^2 p = 0$. We found that each fixed-composition mixture can be considered in a supercritical state above $p = 51$ atm and in particular at $p = 100$ atm. In other words, the instabilities presented in Figure 5 are *not* fixed-composition mechanical instabilities as confirmed by experimental results discussed in the

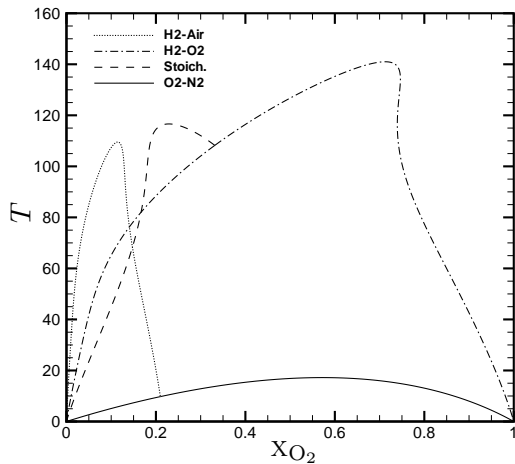


Figure 4: Temperature at thermodynamic stability limits for O_2 -containing mixtures

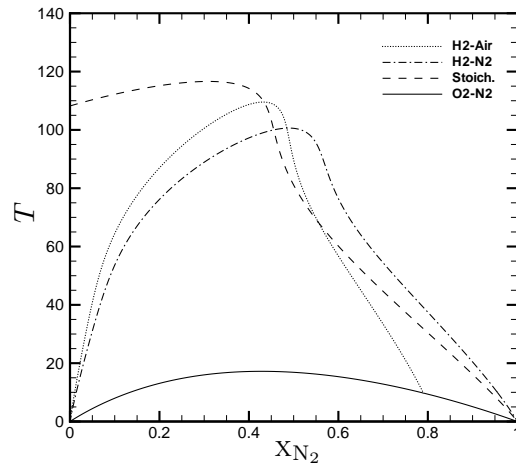


Figure 5: Temperature at thermodynamic stability limits for N_2 -containing mixtures

next section.

5.3 Comparison with experiments

Verschoye [34] and Eubanks [35] have investigated binary mixtures of H_2 and N_2 at high pressure and low temperature. A first important experimental result is that binary mixtures of H_2 and N_2 may not be thermodynamically stable at sufficiently high pressure and low temperature. In these situations, a mixture of H_2 and N_2 splits between a hydrogen-rich gaseous-like phase and a hydrogen-poor liquid-like phase [34, 35] in qualitative agreement with the theoretical results obtained from the SRK equation of state and the eigenvalue analysis of the entropy Hessian matrix $\partial_{\xi\xi}^2 s$ discussed in Section 5.2.

In order to compare quantitatively experimental results with numerical simulations, we have used the data of Eubanks [35]. Since the experiment is at fixed temperature and pressure, it is more natural to consider the Gibbs function $g = h - Ts$ rather than the entropy s . At fixed pressure and temperature the Gibbs function is a convex function of y such that $\partial_{yy}^2 g$ is positive semi-definite and $N(\partial_{yy}^2 g) = \mathbb{R}y$ since $(\partial_{yy}^2 g)/T = \Lambda - \Lambda y \otimes \Lambda y / \langle \Lambda y, y \rangle$ as investigated in Appendix C.

For a given temperature T and pressure p corresponding to experimental measurements, we first computed the two split phases y^\sharp and y^\flat from the SRK equation of state. In order to investigate thermodynamic stability, we present in Figure 6 the profile of a modified specific Gibbs function $g - g^{\text{af}}$ as function of the hydrogen mass fraction Y_{H_2} along the line $y = \alpha y^\sharp + (1 - \alpha)y^\flat$ at temperature $T = 83.15$ K and pressure $p = 95.2$ atm. The values of α insure that the hydrogen mass fraction remains positive. We have subtracted the quantity $g^{\text{af}} = -6.56 \cdot 10^9 - 4.67 \cdot 10^{10} Y_{H_2}$ which is an affine function of Y_{H_2} in order to better emphasize the loss of stability. Figure 6 shows the loss of convexity of Gibbs function and thus of thermodynamic stability along the line passing through y^\sharp and y^\flat . In the zone where the Gibbs function is not anymore convex, the equilibrium limit is given by the convex envelope, obtained here with a segment twice tangent to the curve, and consists in a mixture of the two states y^\sharp and y^\flat associated with the tangency points. We thus observe in Figure 6 a very good agreement between the tangency points y^\sharp and y^\flat represented by squares \square and the experimental measurements of Eubanks represented by diamonds \diamond . On the other hand, the points represented by triangles \triangle correspond to the loss of stability and must be of course within the domain where convexity is loss and within the tangency points. Note that these points \triangle are not exactly inflexion points since the eigenvector associated with the loss

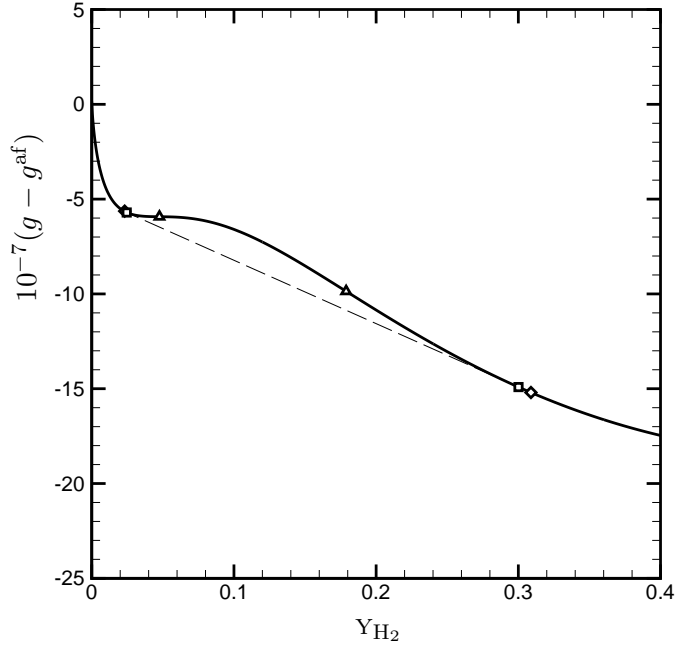


Figure 6: Modified specific Gibbs function as function of the hydrogen mass fraction at $T = 83.15$ K and $T = 95.2$ atm; — Gibbs function curve; □ calculated split phases, ◇ measured split phases, Δ calculated stability limits.

of stability is not necessarily the direction of the line $y^b - y^\sharp$. Between the tangency points (◇) and the stability points (Δ) the mixture is only meta-stable. That is, small perturbations do not change the meta-stable equilibrium but with a large perturbation the system jumps to its convex envelope and split between the two mixtures associated with the tangency points.

The calculation of the two split phases y^\sharp and y^b has been performed by integrating the system of ordinary differential equations

$$\left\{ \begin{array}{l} d_t p^\sharp = 0, \\ d_t n_i^\sharp = \kappa_i (\exp(\mu_i^b) - \exp(\mu_i^\sharp)), \quad i \in \{\text{H}_2, \text{N}_2\}, \\ d_t T^\sharp = 0, \\ d_t p^b = 0, \\ d_t n_i^b = \kappa_i (\exp(\mu_i^\sharp) - \exp(\mu_i^b)), \quad i \in \{\text{H}_2, \text{N}_2\}, \\ d_t T^b = 0, \end{array} \right.$$

where \sharp and b are the indexes of the split phases. The initial conditions must insure that $T^\sharp = T^b = T$ and $p^\sharp = p^b = p$ and it is easily established that $n_i^\sharp + n_i^b$ remains constant for all $i \in \{\text{H}_2, \text{N}_2\}$. This system corresponds to the chemical reaction mechanism $\mathcal{M}_i^\sharp \rightleftharpoons \mathcal{M}_i^b$, $i \in \{\text{H}_2, \text{N}_2\}$, where each species \mathcal{M}_i , $i \in \{\text{H}_2, \text{N}_2\}$, is exchanged between the two phases \sharp and b . Defining $\mathcal{G} = \sum_{i \in \{\text{H}_2, \text{N}_2\}} (n_i^\sharp \mu_i^\sharp + n_i^b \mu_i^b)$ it is easily established that

$$d_t \mathcal{G} = - \sum_{i \in \{\text{H}_2, \text{N}_2\}} (\exp(\mu_i^b) - \exp(\mu_i^\sharp)) (\mu_i^b - \mu_i^\sharp), \quad (64)$$

so that at equilibrium we have $\mu_i^\sharp = \mu_i^b$, $i \in \{\text{H}_2, \text{N}_2\}$, or equivalently, $g_i^\sharp = g_i^b$, $i \in \{\text{H}_2, \text{N}_2\}$. The constants κ_i , $i \in \mathcal{S}$, are the symmetric change of phase constants of the species. Numerically, these constants are taken to be large numbers since we are only interested in the equilibrium limit obtained for $t \rightarrow \infty$.

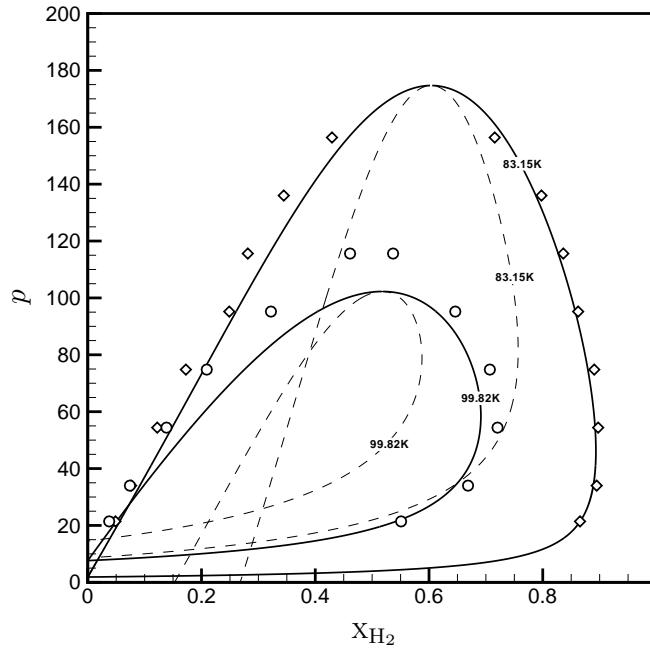


Figure 7: Hydrogen mole fractions of split phases at $T = 83.15$ K and $T = 99.82$ K; — calculated split phases, \diamond measured split phases at $T = 83.15$ K, \circ measured split phases at $T = 99.82$ K, - - - calculated stability limits.

In Figure 7 are presented experimental stability diagrams for $\text{H}_2\text{-N}_2$ mixtures at $T = 83.15$ K and $T = 99.82$ K in the plane (x_{H_2}, p) . The solid lines correspond to the two split phases obtained by continuation techniques and the dash lines correspond to the stability limits obtained by similar techniques. The symbols \diamond correspond to the hydrogen mole fractions of the two split phases at $T = 83.15$ K and the symbols \circ to the hydrogen mole fractions of the two split phases at $T = 99.82$ K as measured by Eubanks [35]. The gaseous-like one on the right is rich in hydrogen whereas the liquid-like one on the left is poor in hydrogen and rich in nitrogen [34, 35]. We observe an excellent agreement for $T = 83.15$ K and a rather good agreement for $T = 99.82$ K. These equilibrium points are very sensitive to temperature and for $T = 97.5$ K instead of $T = 99.82$ K the agreement is again very good. Moreover, the stability limits where the entropy Hessian Λ has a first zero eigenvalue are well within the measured hydrogen mole fractions of both split phases. Overall, considering the simplicity of the SRK equation of state and the fact that there are no adjustable parameters, the agreement with experiment is very good. It is thus remarkable that the high pressure fluid model compares favorably with experiments at high pressure and low temperature as well as for large v or large T where we recover the perfect gas model.

6 Transcritical flame structure

We discuss in this section the structure of transcritical flames and perform a sensitivity analysis with respect to the model. All computed flames are anchored by the condition $T(x^{\text{fx}}) = T^{\text{fx}}$ at $x^{\text{fx}} = 1$ cm with $T^{\text{fx}} = 500$ K. In the next section, we will analyze the influence of various parameters associated with the fresh mixture. Note that, to the authors' knowledge, there are no available experimental data on transcritical—or even supercritical—plane flames.

6.1 Flame structure

We first discuss the structure of a H₂-Air flame with $\varphi = 1$ and $T^{\text{fr}} = 100$ K where φ denotes the equivalence ratio. The dense fluid model presented in Section 2 and Section 3 is used in the calculation with real gas thermodynamics, nonideal transport, density dependent transport coefficients, as well as nonideal chemical productions rates. Figure 8 shows the temperature T , density ρ and mole fractions X_i , $i \in \mathcal{S}$, profiles as function of the flame normal coordinate x . The general structure of H₂-Air low pressure flames has been investigated in particular by Smooke et al. [84], J. Warnatz [85], and F. A. Williams [86]. Since the pressure is of $p = 100$ atm, the resulting flame front is much thinner than at atmospheric pressure [84, 85, 86]. The flame front is roughly 40 μm wide and presents large density gradients due to the cold fresh gas temperature $T^{\text{fr}} = 100$ K and to the combustion heat release. The mass flow rate is found to be $m = 0.981$ g cm⁻² s⁻¹ and the flame speed of $u_{\text{ad}} = 1.866$ cm s⁻¹.

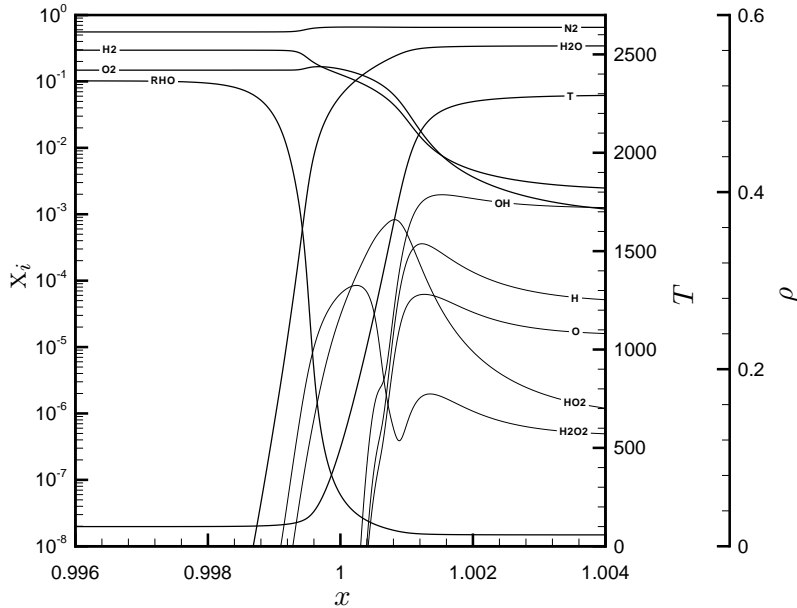


Figure 8: Structure of a transcritical stoichiometric H₂-Air flame with $T^{\text{fr}} = 100$ K and $p = 100$ atm. Density (g cm⁻³), temperature (K) and species mole fractions as functions of spatial coordinate (cm)

In H₂-Air flames, the HO₂ radical is generally formed early in the flame front by the reaction $\text{H} + \text{O}_2 + \text{M} \rightarrow \text{HO}_2 + \text{M}$ until it is dominated by the reaction $\text{H} + \text{O}_2 \rightarrow \text{OH} + \text{O}$ at sufficiently high temperatures [85]. The HO₂ radical is then consumed through its reactions with more active radicals like H or OH. In high pressure flames, however, the reaction $\text{H} + \text{O}_2 + \text{M} \rightarrow \text{HO}_2 + \text{M}$, which decreases the number of moles, dominates $\text{H} + \text{O}_2 \rightarrow \text{OH} + \text{O}$ over a larger temperature domain thanks to the Le Chatellier effect. More specifically, the crossing temperature is around 1400 K for atmospheric flames and around 2100 K at $p = 100$ atm. A remarkable feature of high pressure H₂-Air flames is thus the high concentrations of the HO₂ radical as also discussed by El Gamal et al. [5]. Large concentrations of the H₂O₂ radical are subsequently obtained mainly through the reactions $\text{HO}_2 + \text{HO}_2 \rightarrow \text{H}_2\text{O}_2 + \text{O}_2$ and $\text{H}_2\text{O} + \text{HO}_2 \rightarrow \text{H}_2\text{O}_2 + \text{OH}$ and the radical H₂O₂ peaks before the radical HO₂.

6.2 Influence of the equation of state

We investigate in this section the influence of the equation of state on the structure of the H₂-Air flame presented in Section 6.1. Since the pressure $p = 100$ atm is above the critical pressure of

the reactants H_2 , O_2 , and N_2 , and since the fresh gas temperature $T^{\text{fr}} = 100 \text{ K}$ is lower than the critical temperature of both nitrogen and oxygen, real gas effects are expected to be important in these conditions. The flame structure of Section 6.1, computed with the SRK equation of state, is compared to the similar flame computed with the perfect gas equation of state. The corresponding temperature and density profiles are presented in Figure 9.

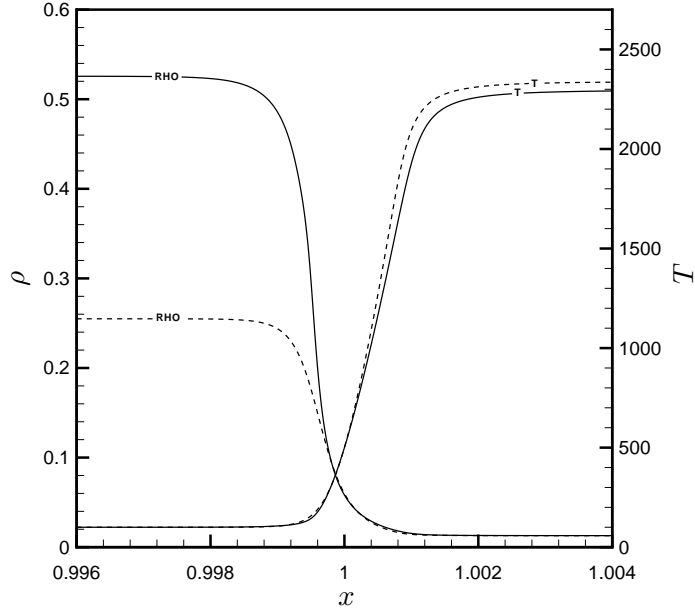


Figure 9: Influence of the state law on the structure of a stoichiometric H_2 -Air flame with $T^{\text{fr}} = 100 \text{ K}$ and $p = 100 \text{ atm}$; Density (g cm^{-3}) and temperature (K) profiles; — : SRK; - - - : PG

Figure 9 shows the dramatic difference between the density of the fresh mixture predicted by the perfect gas equation of state $\rho^{\text{fr,PG}} = 0.255 \text{ g cm}^{-3}$ and the one predicted by the SRK equation of state $\rho^{\text{fr}} = 0.525 \text{ g cm}^{-3}$. The pure component densities at this temperature and pressure are respectively 1.116 g cm^{-3} for O_2 , 0.734 g cm^{-3} for N_2 , and 0.0232 g cm^{-3} for H_2 . An ideal mixing model—even using these values—would further yield a mixture density of 0.401 g cm^{-3} which also differs significantly from the density predicted by the SRK equation of state.

We further observe a modification of the equilibrium temperature when real gas effects are taken into account. The equilibrium state at $+\infty$ is indeed the unique chemical equilibrium point such that $h^{\text{eq}} = h^{\text{fr}}$, $p^{\text{eq}} = p$, $\tilde{Y}_{\text{H}}^{\text{eq}} = \tilde{Y}_{\text{H}}^{\text{fr}}$, $\tilde{Y}_{\text{O}}^{\text{eq}} = \tilde{Y}_{\text{O}}^{\text{fr}}$, and $\tilde{Y}_{\text{N}}^{\text{eq}} = \tilde{Y}_{\text{N}}^{\text{fr}}$. We have denoted here by \tilde{Y}_{H} , \tilde{Y}_{O} , \tilde{Y}_{N} , the atom mass fractions of the elements H, O, and N, respectively, by $^{\text{eq}}$ the superscript associated with the equilibrium state at $+\infty$, and by $^{\text{fr}}$ the superscript associated with the fresh mixture state at $-\infty$. Therefore, the equilibrium point at $+\infty$ depends on thermodynamic properties and is thus modified by nonidealities.

6.3 Influence of transport nonidealities

The influence of transport nonidealities is now investigated by comparing the flame structure of Section 6.1 computed with $d_j = x_j(\mu_j)'_T$ with the flame structure computed with $d_j = x'_j$ as for ideal mixtures. In other words, the flame structure of Section 6.1 which takes into account the full matrix Γ associated with nonidealities is compared with a flame where Γ is replaced by the identity matrix Γ^{PG} . The corresponding temperature T , density ρ and mole fractions X_i , $i \in \mathcal{S}$, profiles are presented in Figure 10 as function of the flame normal coordinate x . We can see at once on Figure 10 that the full transport model prevents the migration of light H_2 toward

the flame front. The same behavior is also observed for the heavier molecules O_2 and N_2 . This hindering of mass diffusion in the dense part of the flame leads to steeper gradients for hydrogen in the flame front and the mixture loses this impermeability only by warming.

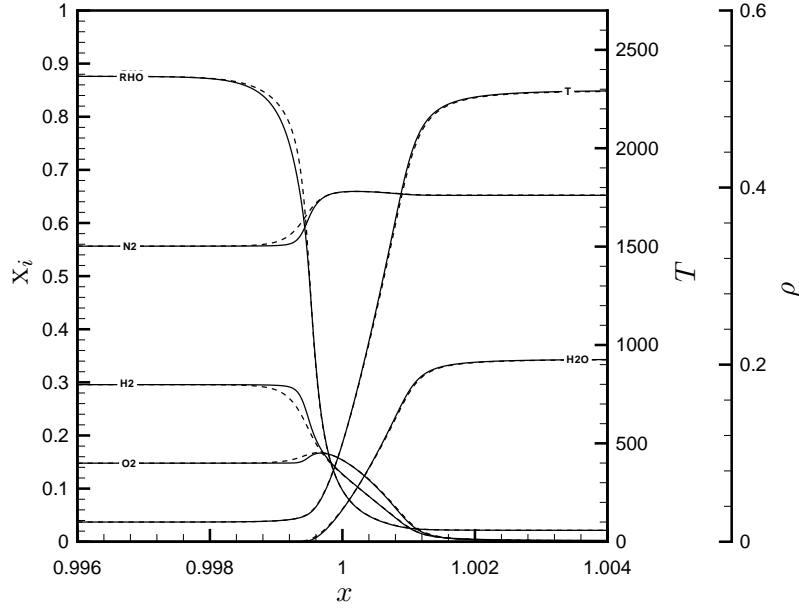


Figure 10: Influence of transport nonidealities on the structure of a stoichiometric H_2 -Air flame with $T^{\text{fr}} = 100$ K and $p = 100$ atm; Density (g cm^{-3}), temperature (K), and mole fraction profiles; — : $\nabla\mu_i$; - - : ∇X_i

To gain more insight into diffusive processes, we present in Figure 11 the contributions to the overall diffusion force d_i of the ideal part ∇X_i and of the nonideal part $X_i(\mu_i^{\text{sm}})'_T$ for the species H_2 and O_2 , and we also plotted the Soret term $\chi_i(\log T)'$. The nonideal contributions $X_i(\mu_i^{\text{sm}})'_T$ are strongly bound to density gradients and are negligible out of a narrow domain located early in the flame front. Neither the mole fraction gradient ∇X_i nor the Soret term $\chi_i(\log T)'$ are confined in this high density region as can be seen for the species O_2 and H_2 in Figure 11. The main effect of the nonideal parts of the diffusion forces seems to hinder mass diffusion between the denser liquid-like region and the flame front. The impact of transport nonidealities may thus even be stronger when the temperature and density profiles stiffen.

The influence of thermal diffusion is analyzed in Figure 12 where the flame structure of Section 6.1 is compared to the analogous flame structure computed without thermal diffusion effects. As for low pressure flames, we observe that, with the Soret effect, the heavy species are more prone to stay in cold zones and the light species try to reach the hotter zones. The species that are mostly influenced are H_2 , N_2 and O_2 as for atmospheric flames [67, 68].

6.4 Influence of transport coefficients

We analyze in this section the impact of the density dependence of transport coefficients expected to be important for transcritical flames. Figure 2 indeed shows that the thermal conductivity of liquid-like states is much greater than the one given by the kinetic theory of dilute gases. We compare in Figure 13 the flame structure of Section 6.1 computed with the Chung high pressure thermal conductivity with the flame structure computed with the dilute gas thermal conductivity. We can see in Figure 13 the enhancement of heat penetration in the dense cold zone leading to smoother density gradients. This is a direct consequence of the much larger thermal conductivity of dense states. The corresponding species mole fraction profiles are also modified and this effect

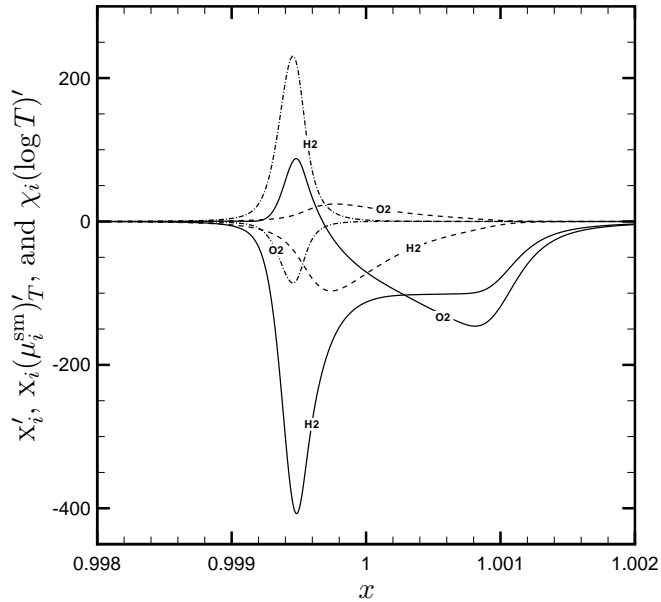


Figure 11: Diffusion driving force terms : — : X'_i ; - - - : $X_i \nabla \mu_i^{sm}$; - · - : $\chi_i(\log T)'$

partially compensates the effect of transport nonidealities.

We compare in Figure 14, the flame structure obtained with the dilute gas binary diffusion coefficients with the flame structure of Section 6.1 computed with high pressure binary thermal diffusion coefficients. The temperature T , density ρ and some mole fractions X_i , $i \in \mathcal{S}$, profiles are presented as function of the flame normal coordinate x . The influence of high pressure corrections to binary diffusion coefficient takes place in a narrow zone between the dense fluid region and the flame front as can be seen for the species H_2O , HO_2 , and H_2O_2 . The other species are mostly absent from this zone and are essentially not modified.

Table 2: Influence of the thermodynamic and transport models on the flame speed

Flame type	EOS	Transport model				Flow rate	Flame speed
H ₂ -Air	SRK	\mathcal{D}_{ij}	λ	χ_i	$\nabla \mu_i$	0.981	1.866
H ₂ -Air	PG	\mathcal{D}_{ij}	λ	χ_i	$\nabla \mu_i$	1.263	4.957
H ₂ -Air	SRK	$\mathcal{D}_{ij}^{\text{dil}}$	λ^{dil}	χ_i	∇X_i	0.965	1.836
H ₂ -Air	SRK	\mathcal{D}_{ij}	λ^{dil}	χ_i	$\nabla \mu_i$	0.977	1.858
H ₂ -Air	SRK	\mathcal{D}_{ij}	λ	0	$\nabla \mu_i$	0.976	1.856

The influence of the thermodynamic and transport models on flame speed is summarized in Table 2. The greatest influence on the flame speed is that of the equation of state. The other effects, although they may change the temperature and species profiles, only influence the flame speed within a few percents.

6.5 Influence of the chemistry model

In a laminar flame, chemical production is mostly significant in a high temperature zone around the flame front. As a consequence, the influence of reaction rates nonidealities is expected to be weak on planar flames unless the pressure is sufficiently high. This is exemplified in Figures 15 and 16 where the rates of progress of the Reaction $\text{OH} + \text{H}_2 \rightleftharpoons \text{H}_2\text{O} + \text{H}$ are plotted at $p = 100$ atm and $p = 1000$ atm, respectively, for the four chemistry models described in Section 4.4.

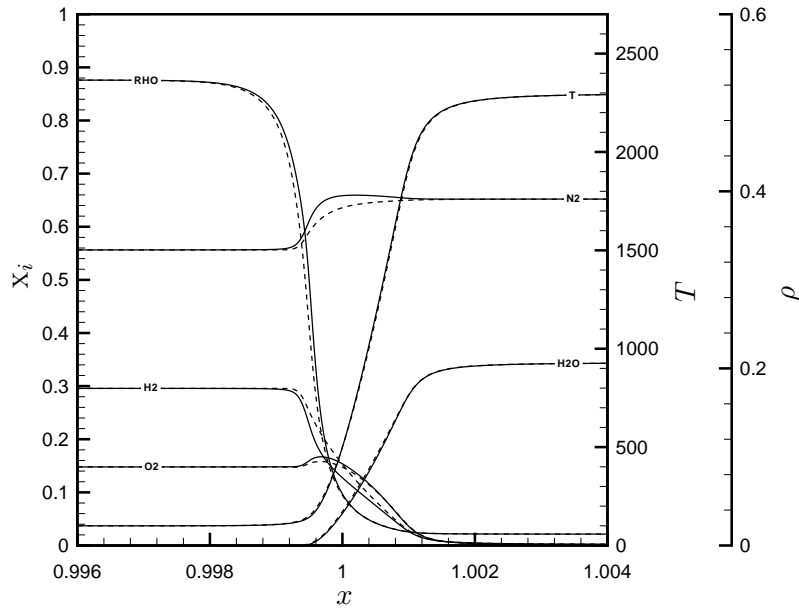


Figure 12: Influence of thermal diffusion on the structure of a stoichiometric H₂-Air flame with $T^{\text{fr}} = 100$ K and $p = 100$ atm; Density (g cm^{-3}), temperature (K), and mole fraction profiles; — : Thermal diffusion included; - - - : Thermal diffusion suppressed

Table 3: Influence of the chemistry model on flame speed at $p = 100$ atm

Flame type	EOS	Chemistry model	Flow rate	Flame speed
H ₂ -Air	SRK	Nonideal	0.981	1.866
H ₂ -Air	SRK	PG	0.979	1.862
H ₂ -Air	SRK	PG - HP	0.977	1.858
H ₂ -Air	SRK	Hybrid	0.972	1.850

In Figure 15 the rates of progress are evaluated for the flame structure of Section 6.1 and in Figure 16 they are evaluated for the analogous flame structure at $p = 1000$ atm. We found it more convenient to plot the various rates of progress for a given flame structure, at each pressure, in order to avoid the small spatial translations obtained when the flame is recalculated for each rate. We have used Reaction 3 of the chemical mechanism since the corresponding rates are large and we remind that the various rates of progress are detailed in Section 4.4. We observe that the influence of nonidealities is still weak at $p = 100$ atm but is very strong at $p = 1000$ atm. It is interesting to note that the worse rates of progress are obtained with the chemistry models PG-HP and Hybrid. In other words, the perfect gas model is closer to the nonideal model than the ‘intermediate’ models. The corresponding flame velocities and mass flow rates are presented in Tables 3 and 4. The influence is weak at $p = 100$ atm but is strong at $p = 1000$ atm with a 25% increase in flame speed between the Hybrid and the Nonideal models.

7 Dependence on initial reactants

We investigate in this section how transcritical flame structures depend on various parameters associated with the incoming fresh mixture.

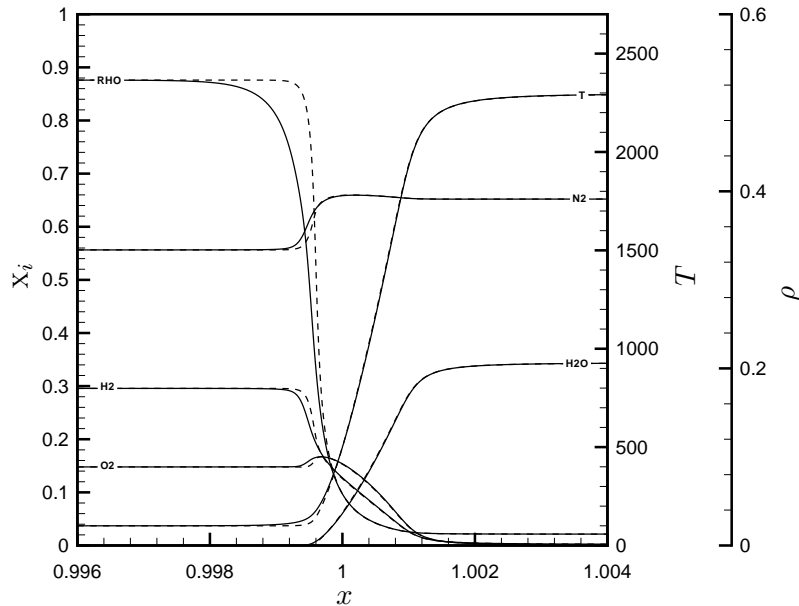


Figure 13: Influence of thermal conductivity on the structure of a stoichiometric H₂-Air flame with $T^{\text{fr}} = 100$ K and $p = 100$ atm; Density (g cm^{-3}), temperature (K), and mole fraction profiles; — : high pressure coefficient λ ; - - - : dilute gas coefficient λ^{dil}

Table 4: Influence of the chemistry model on the flame speed at $p = 1000$ atm

Flame type	EOS	Chemistry model	Flow rate	Flame speed
H ₂ -Air	SRK	Nonideal	4.007	5.449
H ₂ -Air	SRK	PG	3.652	4.966
H ₂ -Air	SRK	PG - HP	3.292	4.476
H ₂ -Air	SRK	Hybrid	3.227	4.389

7.1 Influence of the equivalence ratio

In order to evaluate the influence of the equivalence ratio φ on H₂-Air flames, we have computed a lean flame with $\varphi = 0.6$, $T^{\text{fr}} = 100$ K and $p = 100$ atm. The corresponding flame structure is presented in Figure 17.

Compared to the stoichiometric flame structure described in Figure 8 the flame is much thicker and the flame front is 0.7 mm wide. The flame is also cooler with the maximum temperature reduced by 700 K. The OH radical also presents a much higher concentration than H which nearly disappears at equilibrium, unlike with the stoichiometric flame. The importance of the HO₂ and H₂O₂ radicals is even more pronounced than for the stoichiometric flame since now the reaction $\text{H} + \text{O}_2 + \text{M} \rightarrow \text{HO}_2 + \text{M}$ *always* dominate the reaction $\text{H} + \text{O}_2 \rightarrow \text{OH} + \text{O}$. The radical H₂O₂ is formed through the reactions $\text{HO}_2 + \text{HO}_2 \rightarrow \text{H}_2\text{O}_2 + \text{O}_2$, $\text{HO}_2 + \text{H}_2 \rightarrow \text{H}_2\text{O}_2 + \text{H}$, and $\text{H}_2\text{O} + \text{HO}_2 \rightarrow \text{H}_2\text{O}_2 + \text{OH}$ and peaks before the radical HO₂.

7.2 Influence of the dilution ratio

In order to investigate the influence of the dilution ratio, we have computed a stoichiometric H₂-O₂ transcritical flame. The ambient pressure is still of $p = 100$ atm but for thermodynamic stability reasons the fresh gas temperature is $T^{\text{fr}} = 110$ K and the corresponding flame structure is presented in Figure 18. The mass flow rate is found to be $m = 44.64$ g cm⁻² s⁻¹ and the flame

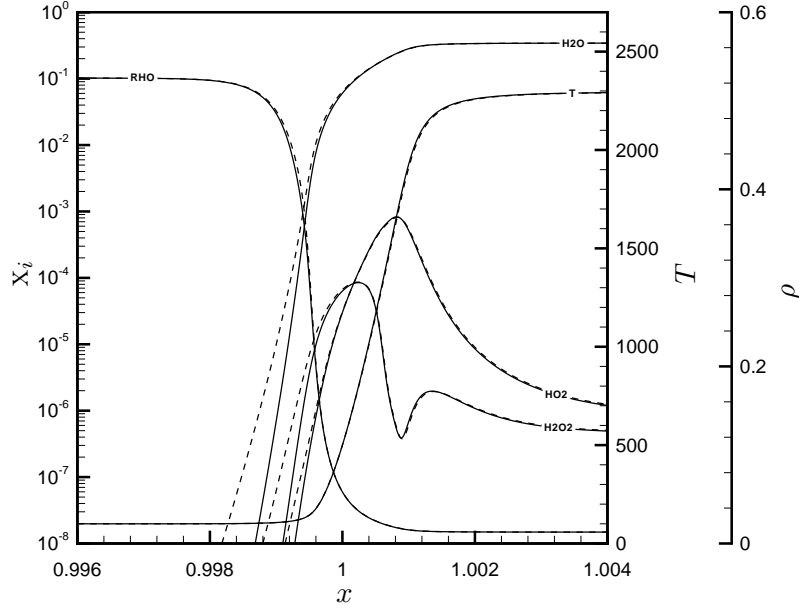


Figure 14: Influence of binary diffusion coefficients on the structure of a stoichiometric H₂-Air flame with $T^{\text{fr}} = 100$ K and $p = 100$ atm; Density (g cm^{-3}), temperature (K), and mole fraction profiles; — : high pressure coefficient \mathcal{D}_{ij} ; - - - : dilute gas coefficient $\mathcal{D}_{ij}^{\text{dil}}$

speed $u_{\text{ad}} = 253.3 \text{ cm s}^{-1}$.

The higher flame speed and flow rate are responsible for the steeper gradients in the flame and the flame front thickness is about $1 \mu\text{m}$. Another important difference with the H₂-Air stoichiometric case is the much higher maximum gas temperature, as it is for low pressure flames. Thanks to this higher temperature, the radicals H, O, and OH are in much higher concentrations than the radicals HO₂ and H₂O₂, at variance with H₂-Air flames where the reaction $\text{H} + \text{O}_2 + \text{M} \rightarrow \text{HO}_2 + \text{M}$ mostly dominates $\text{H} + \text{O}_2 \rightarrow \text{OH} + \text{O}$. Indeed, the maximum temperature around 3800 K is well above the crossing temperature 2100 K at $p = 100$ atm.

7.3 Lean and rich extinction limits

We investigate in this section the flammability domains of H₂-Air and H₂-O₂ flames in the plane (φ, T^{fr}) where φ denotes the equivalence ratio and T^{fr} the fresh gas temperature at $p = 100$ atm.

Combustion theory has established that heat losses are required in order to obtain turning points with respect to the equivalence ratio φ and well defined extinction limits even though the precise form of the heat loss rate is not significant [86, 87, 88]. In order to investigate composition extinction limits, radiative volumetric heat losses to the surroundings have been added to the energy equation in the form

$$mh' + q' = -\mathcal{H}, \quad (65)$$

where \mathcal{H} denotes the heat loss term. The radiative heat loss term \mathcal{H} is modeled by assuming an optically thin transfer between the fluid and the cold surroundings and reads

$$\mathcal{H} = \begin{cases} 4\bar{\sigma} p_{\text{H}_2\text{O}} c_{\text{H}_2\text{O}} (T^4 - T_0^4), & \text{if } T \geq T_0, \\ 0, & \text{otherwise,} \end{cases} \quad (66)$$

where $\bar{\sigma}$ denotes the Stefan-Boltzmann constant, $p_{\text{H}_2\text{O}}$ the partial pressure of H₂O, $c_{\text{H}_2\text{O}}$ the Planck mean absorption coefficient for H₂O, and T_0 an ambient temperature towards which the combustion products ultimately relax. The Planck mean absorption coefficient of H₂O is modeled

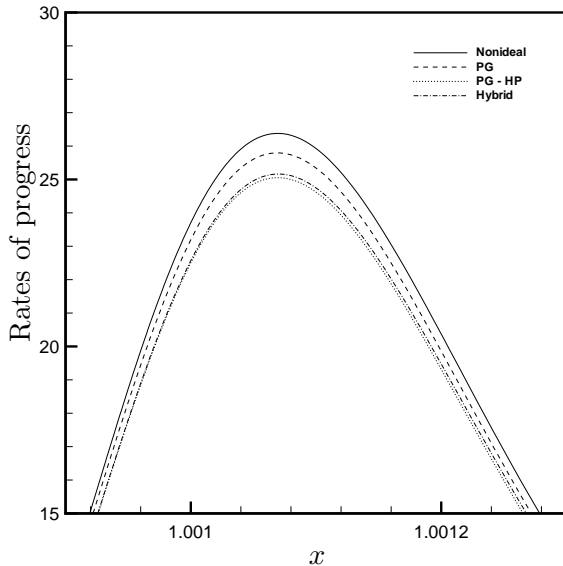


Figure 15: Rates of progress of Reaction $\text{OH} + \text{H}_2 \rightleftharpoons \text{H}_2\text{O} + \text{H}$ for various chemistry models at 100 atm

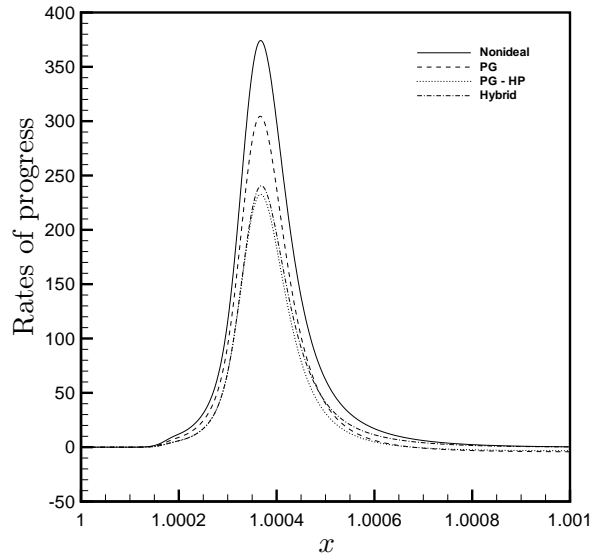


Figure 16: Rates of progress of Reaction $\text{OH} + \text{H}_2 \rightleftharpoons \text{H}_2\text{O} + \text{H}$ for various chemistry models at 1000 atm

as a polynomial in temperature [89]. The choice of the temperature T_0 is not as straightforward as for ideal mixtures since mixtures rich in H_2O —as combustion products in a Hydrogen flame—may not be thermodynamically stable at pressure $p = 100$ atm. More specifically, it is forbidden to choose a temperature T_0 below the thermodynamic stability limit of the combustion products. To prevent this phenomenon we have used a rather high ambient temperature of $T_0 = 650$ K, which insures the super-criticality of water in the burnt gases and forbids unstable states in the wake of the flame.

Typical extinction diagrams are presented on Figure 19 for H_2 -Air flames and on Figure 20 for H_2 - O_2 flames, with $T^{\text{fr}} = 100, 150, 200, 250, 300$ K and $p = 100$ atm. We observe typical bell-shaped curves [80, 88] with two turning points. The lean extinction limit is on the left and the rich extinction limit on the right. Various tests have shown that the position of these turning points is insensitive to the precise form of the heat loss rate as for dilute gases [86]. The most inner curves correspond to the lowest temperature. Note that, contrarily to usual diagrams, the upper part of these curves are not closed for $T^{\text{fr}} = 100$ K since they cross the thermodynamic stability limit of the fresh gases.

The flammability domains in the (φ, T^{fr}) plane are presented in Figure 21 for H_2 -Air flames and Figure 22 for H_2 - O_2 flames. These figures show the influence of the fresh gases temperature T^{fr} on the localization of the lean and rich extinction limits. In addition, the whole (φ, T^{fr}) domain is not accessible and the flammability domain is bounded from below by the thermodynamic stability limit of the injected mixture for H_2 -Air and H_2 - O_2 flames. There are also rare situations where some mixture states within the flame are unstable due to species diffusion from the flame front into the cold preheat zone. This situation only occurs for lean H_2 - O_2 flames with equivalence ratios around 0.15–0.2.

8 Conclusion

A detailed high pressure flame model has been derived from macroscopic and/or molecular theories and the corresponding entropy production has been shown to be nonnegative. Using the SRK equation of state, we have established that at sufficiently low temperatures, fresh mixtures of H_2 - O_2 - N_2 flames are thermodynamically unstable, as confirmed by experimental results. The

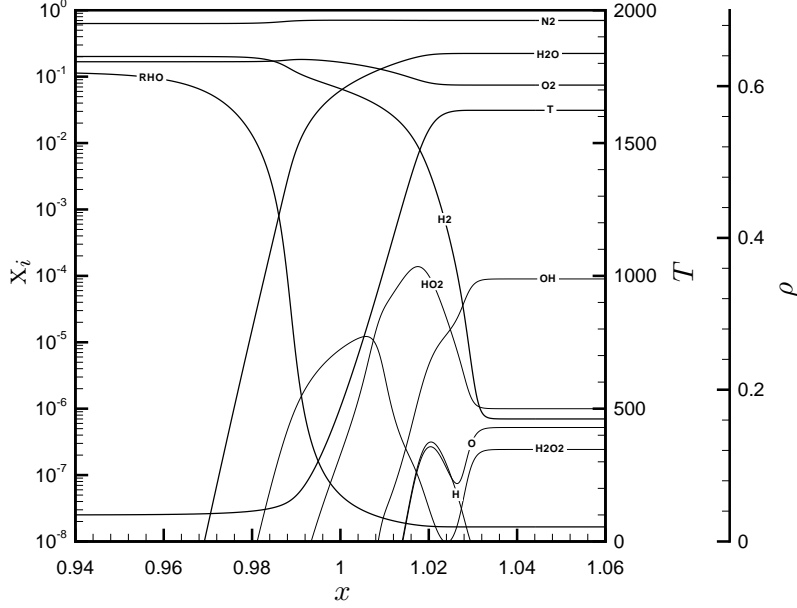


Figure 17: Structure of a transcritical lean H_2 -Air flame with $\varphi = 0.6$, $T^{\text{fr}} = 100$ K and $p = 100$ atm. Density (g cm^{-3}), temperature (K) and species mole fractions as functions of spatial coordinate (cm)

structure of planar transcritical H_2 - O_2 - N_2 flames has been analyzed and we have performed a sensitivity analysis with respect to the model. Nonidealities in the equation of state and in the transport fluxes have a strong influence on the cold part of the flame as well as the dependence of thermal conductivity on density. Finally, we have established that the flammability domain in the plane (φ, T^{fr}) is bounded on the left by the lean extinction curve, on the right by the rich extinction curve, and at the bottom by the thermodynamic stability limit of the fresh mixture. To the authors' knowledge, it is the first time that such flammability domains bounded by thermodynamic limits are presented.

A Thermodynamic properties

The determination of thermodynamics properties of a gas following a SRK equation of state is based on the determination of its Helmholtz free energy f . This thermodynamical function f is easily expressed in terms of the pressure deviation $\phi = p - p^{\text{PG}}$ and the perfect gas free energy f^{PG}

$$f(v, Y_1, \dots, Y_{n^e}, T) = f^{\text{PG}}(v, Y_1, \dots, Y_{n^e}, T) + \int_v^\infty \phi(v', Y_1, \dots, Y_{n^e}, T) dv'. \quad (67)$$

Using then the SRK equation of state, the previous expression yields

$$f = \sum_{i \in \mathcal{S}} Y_i f_i^{\text{PG}\star} + \sum_{i \in \mathcal{S}} \frac{Y_i}{m_i} RT \ln \left(\frac{Y_i RT}{m_i (v - b) p^{\text{st}}} \right) - \frac{a}{b} \ln \left(1 + \frac{b}{v} \right), \quad (68)$$

where $f_i^{\text{PG}\star} = f_i^{\text{PG}\star}(T)$ denotes the perfect gas specific free energy of the i th species at pressure p^{st} .

The other usual thermodynamical functions are then deduced from the Helmholtz free energy f . More specifically, the mixture entropy s can be obtained from $s = -(\partial f / \partial T)_{v, Y_i}$ and reads

$$s = \sum_{i \in \mathcal{S}} Y_i s_i^{\text{PG}\star} - \sum_{i \in \mathcal{S}} \frac{Y_i}{m_i} R \ln \left(\frac{Y_i RT}{m_i (v - b) p^{\text{st}}} \right) + \frac{\partial_T a}{b} \ln \left(1 + \frac{b}{v} \right), \quad (69)$$

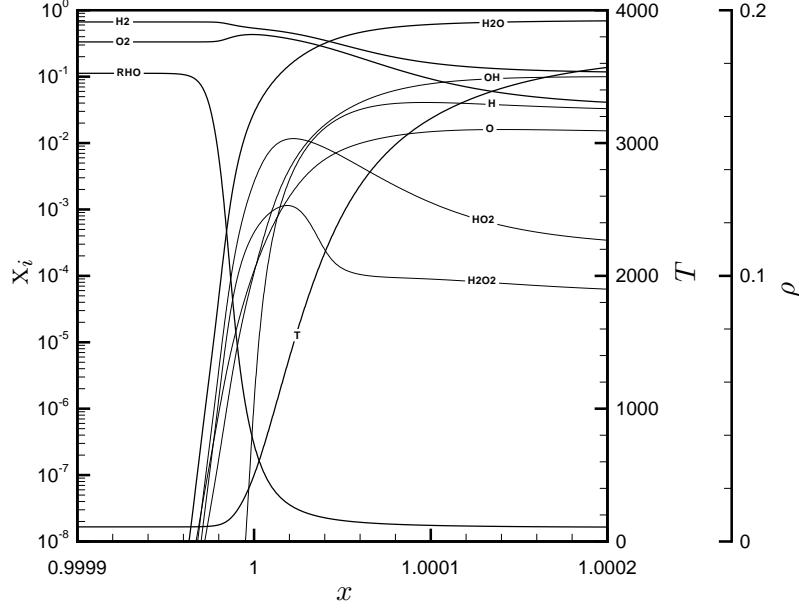


Figure 18: Structure of a transcritical stoichiometric $\text{H}_2\text{-O}_2$ flame with $T^{\text{fr}} = 110$ K and $p = 100$ atm. Density (g cm^{-3}), temperature (K) and species mole fractions as functions of spatial coordinate (cm)

where $e_i^{\text{PG}^*} = s_i^{\text{PG}^*}(T)$ denotes the perfect gas specific entropy of the i th species at pressure p^{st} . The mixture internal energy $e = f + Ts$ is then given by

$$e = \sum_{i \in \mathcal{S}} Y_i e_i^{\text{PG}} + (T \partial_T a - a) \frac{1}{b} \ln\left(1 + \frac{b}{v}\right), \quad (70)$$

where $e_i^{\text{PG}} = e_i^{\text{PG}}(T)$ denotes the perfect gas specific energy of the i th species whereas the enthalpy $h = f + pv$ reads

$$h = \sum_{i \in \mathcal{S}} Y_i h_i^{\text{PG}} + (T \partial_T a - a) \frac{1}{b} \ln\left(1 + \frac{b}{v}\right) + \sum_{i \in \mathcal{S}} \frac{Y_i}{m_i} \frac{RTb}{v - b} - \frac{a}{v + b}, \quad (71)$$

where $h_i^{\text{PG}} = h_i^{\text{PG}}(T)$ denotes the perfect gas specific enthalpy of the i th species. Finally, the Gibbs function $g = f + pv$ is given by

$$\begin{aligned} g &= \sum_{i \in \mathcal{S}} Y_i (h_i^{\text{PG}} - T s_i^{\text{PG}^*}) + \sum_{i \in \mathcal{S}} \frac{Y_i}{m_i} RT \ln\left(\frac{Y_i RT}{m_i (v - b) p^{\text{st}}}\right) \\ &+ \sum_{i \in \mathcal{S}} \frac{Y_i}{m_i} \frac{RTb}{v - b} - \frac{a}{b} \ln\left(1 + \frac{b}{v}\right) - \frac{a}{v + b}. \end{aligned} \quad (72)$$

The thermodynamic properties may also easily be expressed in terms of the species mole fractions x_1, \dots, x_{n^e} defined by

$$x_i = \frac{Y_i m}{m_i}, \quad i \in \mathcal{S}, \quad \frac{\sum_{i \in \mathcal{S}} Y_i}{m} = \sum_{i \in \mathcal{S}} \frac{Y_i}{m_i}, \quad (73)$$

where m is the molar mass of the mixture. Note the factor $\sum_{i \in \mathcal{S}} Y_i$ in the definition of the mixture molar mass m which insures that m is a zero-homogeneous function of the mass or mole

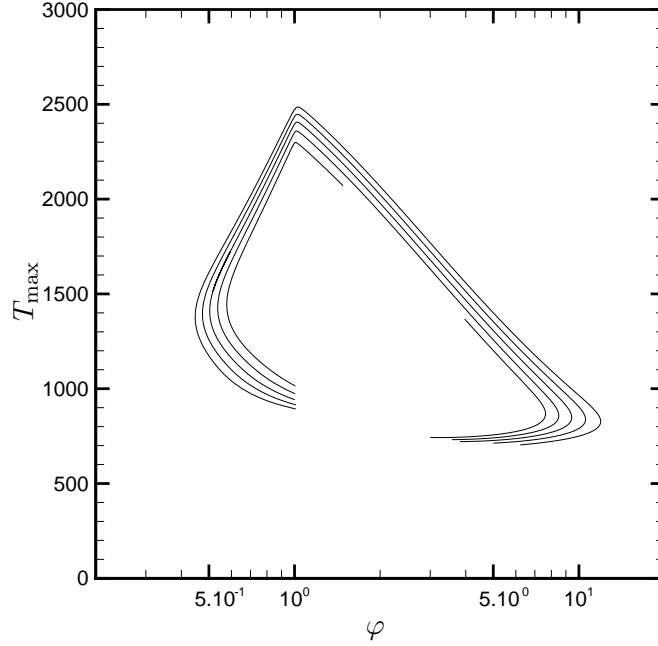


Figure 19: Maximum temperature as function of the equivalence ratio in a H₂-Air flame with $T^{\text{fr}} = 100, 150, 200, 250, 300$ K and $p = 100$ atm. Lower temperatures correspond to more inner curves.

fractions and that the mole/mass relations are invertible [30]. It is easily established in particular that $\sum_{i \in \mathcal{S}} Y_i = \sum_{i \in \mathcal{S}} X_i$ so that

$$Y_i = \frac{X_i m_i}{m}, \quad i \in \mathcal{S}, \quad \left(\sum_{i \in \mathcal{S}} X_i \right) m = \sum_{i \in \mathcal{S}} X_i m_i.$$

B Thermal conductivity

The Chung coefficients β and λ^{hp} used for the evaluation of the thermal conductivity

$$\lambda = \lambda^{\text{dil}} \beta + \lambda^{\text{hp}}, \quad (74)$$

are discussed in this section [70]. The Chung correlation is based on the definition of critical properties of the mixture built on molecular parameters in the following way

$$T_{c,m} = 1.2593 \frac{\epsilon_m}{k}, \quad v_{c,m} = 1.8887 \sigma_m^3, \quad (75)$$

where the Lennard Jones well depth of the mixture ϵ_m is expressed in J, the Boltzmann constant k in J K⁻¹, the mean molecular diameter σ_m in Å, the critical temperature $T_{c,m}$ in K, and the critical volume $v_{c,m}$ in cm³ mol⁻¹. The mean molecular parameters of the mixture are computed from the pure species parameters using mixing rules

$$\sigma_m^3 = \sum_{i,j \in \mathcal{S}} X_i X_j \sigma_{ij}^3, \quad \epsilon_m \sigma_m^3 = \sum_{i,j \in \mathcal{S}} X_i X_j \epsilon_{ij} \sigma_{ij}^3, \quad (76)$$

$$\varpi_m \sigma_m^3 = \sum_{i,j \in \mathcal{S}} X_i X_j \varpi_{ij} \sigma_{ij}^3, \quad m_m^{\frac{1}{2}} \epsilon_m \sigma_m^2 = \sum_{i,j \in \mathcal{S}} X_i X_j m_{ij}^{\frac{1}{2}} \epsilon_{ij} \sigma_{ij}^2, \quad (77)$$

$$\frac{\mu_m^4}{\epsilon_m \sigma_m^3} = \sum_{i,j \in \mathcal{S}} X_i X_j \frac{\mu_i^2 \mu_j^2}{\epsilon_{ij} \sigma_{ij}^3}, \quad \kappa_m = \sum_{i,j \in \mathcal{S}} X_i X_j \kappa_{ij}, \quad (78)$$

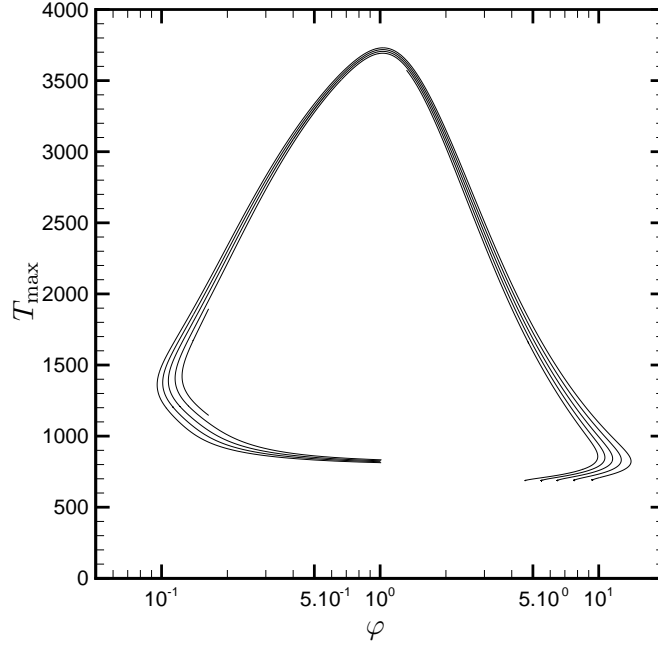


Figure 20: Maximum temperature as function of the equivalence ratio in a H₂-O₂ flame with $T^{\text{fr}} = 100, 150, 200, 250, 300$ K and $p = 100$ atm. Lower temperatures correspond to more inner curves.

where κ_{ij} is the association parameter and μ_i the dipole moment. The species pair parameter are evaluated as $\sigma_{ij} = (\sigma_i \sigma_j)^{\frac{1}{2}}$, $\epsilon_{ij} = (\epsilon_i \epsilon_j)^{\frac{1}{2}}$, $\varpi_{ij} = \frac{\varpi_i + \varpi_j}{2}$, $m_{ij} = \frac{2m_i m_j}{m_i + m_j}$, $\kappa_{ij} = (\kappa_i \kappa_j)^{\frac{1}{2}}$. The association parameter for H₂O is $\kappa_{\text{H}_2\text{O}} = 0.075908$ and is otherwise zero. The thermal conductivity correction β proposed by Chung is then written

$$\beta = \left(\frac{1}{H_2} + B_6 \gamma^* \right), \quad \gamma^* = \gamma \frac{v_{c,m}}{6}. \quad (79)$$

where γ is the number density and γ^* the reduced molar density of the mixture. The high density thermal conductivity λ^{hp} is given, in $\text{cal cm}^{-1} \text{s}^{-1} \text{K}^{-1}$, as

$$\lambda^{\text{hp}} = \left(3.039 \times 10^{-4} \frac{T_{c,m}^{\frac{1}{2}}}{m_m^{\frac{1}{2}} v_{c,m}^{\frac{2}{3}}} \right) B_7 \gamma^{*2} H_2 (T^*)^{\frac{1}{2}}, \quad (80)$$

the reduced temperature T^* being evaluated as $T^* = kT/\epsilon_m$. The H_2 coefficient is computed as

$$H_2 = \frac{B_1(1 - \exp(-B_4 \gamma^*)/\gamma^* + B_2 G_1 \exp(B_5 \gamma^*) + B_3 G_1}{B_1 B_4 + B_2 + B_3}, \quad (81)$$

with $G_1 = (2 - \gamma^*)/(2(1 - \gamma^*)^3)$. The various B_i coefficients are obtained through the parameter correlation

$$B_i = b_0(i) + b_1(i) \varpi_m + b_2(i) \mu_m^4 \frac{131.3^4}{v_{c,m}^2 T_{c,m}^2} + b_3(i) \kappa_m, \quad (82)$$

with the $b_k(i)$ coefficients given in table 5.

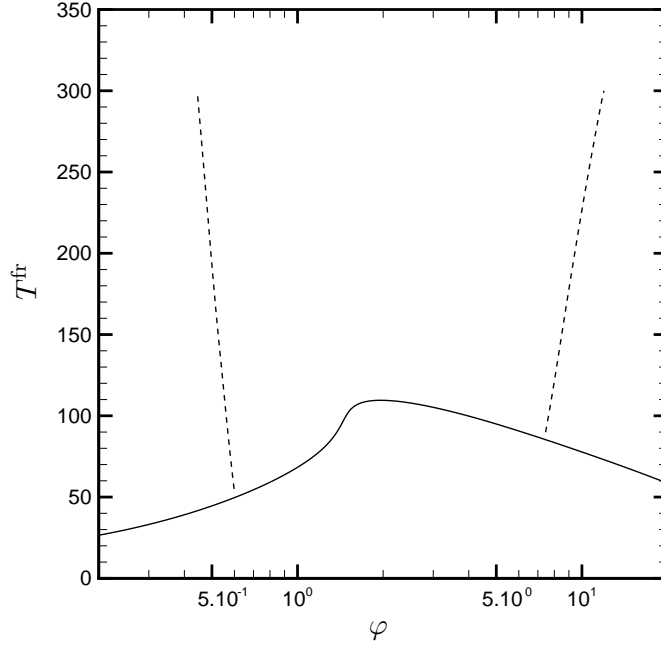


Figure 21: Flammability domain of H_2 -Air flames in the (φ, T^{fr}) plane; - - - lean and rich extinction limits; — fresh mixture thermodynamic stability limit.

Table 5: Coefficient for the evaluation of B_i parameters

i	$b_0(i)$	$b_1(i)$	$b_2(i)$	$b_3(i)$
1	2,41657	0,74824	-0,91858	121,72100
2	-0,50924	-1,50936	-49,99120	69,98340
3	6,61069	5,62073	64,75990	27,03890
4	14,54250	-8,91387	-5,63794	74,34350
5	0,79274	0,82019	-0,69369	6,31734
6	-5,86340	12,80050	9,58926	-65,52920
7	81,17100	114,15800	-60,84100	466,77500

C Entropy hessian and stability

We investigate in this section various properties of the matrix Λ associated with the entropy hessian. We first establish that the relation

$$\sum_{i,j \in \mathcal{S}} Y_i Y_j \Lambda_{ij} = -\frac{v^2}{T} \tilde{\partial}_v p, \quad (83)$$

is a consequence of homogeneity. Since the pressure law is 0-homogeneous with respect to the variable (v, Y_1, \dots, Y_n) , we have the Euler relations

$$\sum_{i \in \mathcal{S}} Y_i \tilde{\partial}_{Y_i} \phi + v \tilde{\partial}_v \phi = 0, \quad (84)$$

and

$$\sum_{i \in \mathcal{S}} Y_i \tilde{\partial}_{Y_i Y_j}^2 \phi + v \tilde{\partial}_{v Y_j}^2 \phi = -\tilde{\partial}_{Y_j} \phi, \quad j \in \mathcal{S}, \quad \sum_{i \in \mathcal{S}} Y_i \tilde{\partial}_{Y_i v}^2 \phi + v \tilde{\partial}_{vv}^2 \phi = -\tilde{\partial}_v \phi. \quad (85)$$

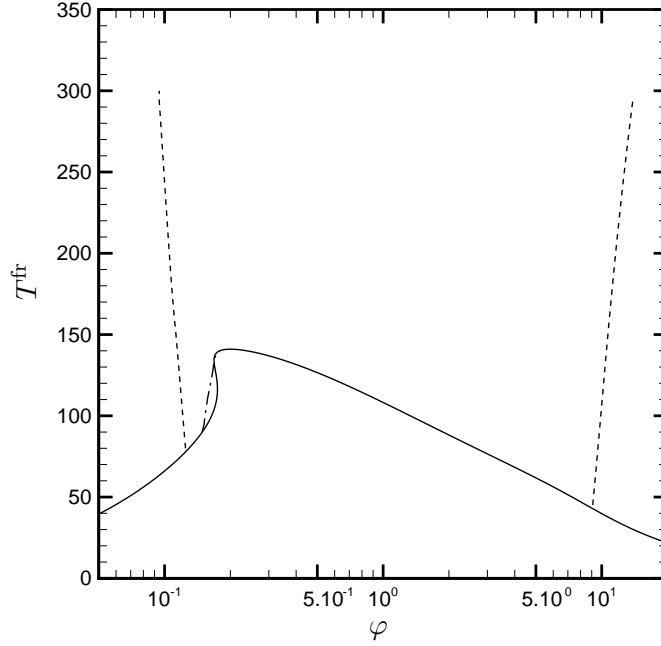


Figure 22: Flammability domain of H₂-O₂ flames in the (φ, T^{fr}) plane; - - - lean and rich extinction limits; — fresh mixture thermodynamic stability limit; - · - preheat zone states thermodynamic limit.

After some algebra, we easily obtain $\sum_{i,j \in \mathcal{S}} Y_i Y_j \tilde{\partial}_{Y_i, Y_j}^2 \phi = \tilde{\partial}_v (v^2 \tilde{\partial}_v \phi)$ and integrating over $(v, +\infty)$ we get

$$\int_v^\infty \sum_{i,j \in \mathcal{S}} Y_i Y_j \tilde{\partial}_{Y_i, Y_j}^2 \phi dv' = -v^2 \tilde{\partial}_v \phi, \quad (86)$$

since $\phi \sim v^{-2}$ and $\tilde{\partial}_v \phi \sim v^{-3}$ for large v so that $\lim_{v \rightarrow \infty} (v^2 \tilde{\partial}_v \phi) = 0$. Equation (83) is then a consequence of $\Lambda_{ij} = \frac{R}{m_i Y_i} \delta_{ij} + \frac{1}{T} \int_v^\infty \tilde{\partial}_{Y_i, Y_j}^2 \phi dv'$, $\sum_{i \in \mathcal{S}} \frac{R Y_i}{m_i} = -\frac{v^2}{T} \tilde{\partial}_v p^{\text{PG}}$ and $p = p^{\text{PG}} + \phi$.

In the case of a Soave-Redlich-Kwong equation of state with Van der Waals mixing rules, the coefficients Λ_{ij} can be further evaluated analytically

$$\begin{aligned} \Lambda_{ij} = & \frac{R \delta_{ij}}{m_i Y_i} + \frac{R}{v-b} \left(\frac{b_i}{m_j} + \frac{b_j}{m_i} \right) + \sum_{k \in \mathcal{S}} \frac{Y_k}{m_k} \frac{R}{(v-b)^2} b_i b_j - \frac{2}{T} \frac{a_{ij}}{b} \ln \left(1 + \frac{b}{v} \right) \\ & + \frac{2}{T} \sum_{k \in \mathcal{S}} Y_k (a_{ik} b_j + a_{jk} b_i) \left(\frac{1}{b^2} \ln \left(1 + \frac{b}{v} \right) - \frac{1}{b(v+b)} \right) \\ & + \frac{1}{T} a b_i b_j \left(-\frac{2}{b^3} \ln \left(1 + \frac{b}{v} \right) + \frac{2}{b^2(v+b)} + \frac{1}{b(v+b)^2} \right), \quad i, j \in \mathcal{S}. \end{aligned} \quad (87)$$

Finally, the stability condition $c_v > 0$ is easily checked since

$$c_v = c_v^{\text{PG}} + \frac{T \partial_{TT}^2 a}{b} \ln \left(1 + \frac{b}{v} \right), \quad (88)$$

and the Soave temperature dependance insures that $\partial_{TT}^2 a \geq 0$ since $a = \sum_{i,j \in \mathcal{S}} Y_i Y_j a_{ij}$ and $\partial_{TT}^2 a_{ij} \geq 0$. Note that with the exponential form of the temperature coefficient α_i the coefficient c_v is smooth whereas with the Soave form, original or truncated, there are Dirac masses at the crossover temperatures $T_{c,i}(1 + 1/s_i)^2$, $i \in \mathcal{S}$. These Dirac masses usually have a negligible

influence since the temperatures $T_{c,i}(1 + 1/s_i)^2$, $i \in \mathcal{S}$, are large and then nonidealities are generally negligible.

Finally, an explicit calculation establishes that $\partial_{v_i v_j}^2 g = T\Lambda_{ij} + v_i v_j \tilde{\partial}_v p$ and furthermore that $T(\Lambda y)_k = -v_k v \tilde{\partial}_v p$ in such a way that

$$\frac{\partial_{YY}^2 g}{T} = \Lambda - \frac{\Lambda y \otimes \Lambda y}{\langle \Lambda y, y \rangle}.$$

Therefore, we have

$$\frac{\langle (\partial_{YY}^2 g)x, x \rangle}{T} = \left\langle \Lambda \left(x - y \frac{\langle \Lambda x, y \rangle}{\langle \Lambda y, y \rangle} \right), \left(x - y \frac{\langle \Lambda x, y \rangle}{\langle \Lambda y, y \rangle} \right) \right\rangle,$$

and $\partial_{YY}^2 g$ is positive semi-definite with nullspace $\mathbb{R}y$ when Λ is positive definite. Similarly, above the critical pressure, we have $\langle \Lambda y, y \rangle > 0$ and if Λ has a negative eigenvalue, then automatically $\partial_{YY}^2 g$ also has a negative eigenvalue.

References

- [1] W. Schilling and E.U. Franck, *Combustion and diffusion flames at high pressures to 2000 bar*, Ber. Bunseng. Phys. Chem. 92-5 (1988), pp. 631–636.
- [2] B. Chehroudi, D. Talley and E. Coy, *Visual characteristics and initial growth rates of round cryogenic jets at subcritical and supercritical pressures*, Phys. Fluids 14 (2002), pp. 850–861.
- [3] M. Habiballah, M. Orain, F. Grisch, L. Vingert, and P. Gicquel, *Experimental studies of high pressure cryogenic flames on the MASCOTTE facility*, Comb., Sci. Tech. 178 (2006), pp. 101–128.
- [4] S. Candel, M. Juniper, G. Singla, P. Scouffaire, and C. Rolon, *Structure and dynamics of cryogenic flames at supercritical pressure*, Comb. Sci. Tech. 178 (2006), pp. 161–192.
- [5] M. El Gamal, E. Gutheil and J. Warnatz, *The structure of laminar premixed H₂-Air flames at elevated pressures*, Zeit. Phys. Chem. 214 (2000), pp. 419–435.
- [6] A.M. Saur, F. Behrendt, and E.U. Franck, *Calculation of high pressure counterflow diffusion flame up to 3000 bar*, Ber. Buns. Phys. Chem. 97-7 (1993), pp. 900–908.
- [7] G. Ribert, N. Zong, V. Yang, L. Pons, N. Darabiha, and S. Candel, *Counterflow diffusion flames of general fluids: Oxygen/Hydrogen mixtures*, Comb. Flame 154 (2008), pp. 319–330.
- [8] L. Pons, N. Darabiha, S. Candel, G. Ribert, and V. Yang, *Mass transfer and combustion in transcritical non-premixed counterflows*, Comb. Theory Mod. 13-1 (2009), pp. 57–81.
- [9] N. A. Okongo and J. Bellan, *Direct numerical simulation of a transitional supercritical binary mixing layer: heptane and nitrogen*, J. Fluid Mech. 464 (2002), pp. 1–34.
- [10] N. Zong and V. Yang, *Cryogenic fluid jets and mixing layers in transcritical and supercritical environments*, Comb. Sci. Tech. 178 (2006), pp. 193–227.
- [11] J. Bellan, *Theory, modeling and analysis of turbulent supercritical mixing*, Comb. Sci. Tech. 178 (2006), pp. 253–281.
- [12] J.C. Oefelein, *Thermophysical characteristics of shear-coaxial LOX-H₂ flames at supercritical pressure*, Proc. Comb. Inst. 30 (2005), pp. 2929–2937.
- [13] N. Zong and V. Yang, *Near-field flow and flame dynamics of LOX/methane shear-coaxial injector under supercritical conditions*, Proc. Comb. Inst. 30 (2007), pp. 2309–2317.

- [14] T. Schmitt, L. Selle, B. Cuenot, and T. Poinso, *Large eddy simulations of transcritical flows*, *Compte-rendus de l'Académie des Sciences* 1 (2008), pp. 1–2.
- [15] J. Meixner, *Zur Thermodynamik der Thermodiffusion*, *Ann. der Phys.*, 41 (1941), pp. 333–356.
- [16] J. Meixner, *Zur Thermodynamik der irreversiblen Prozesse in Gasen mit chemisch reagierenden, dissoziierenden und anregbaren Komponenten*, *Ann. der Phys.*, 43 (1943), pp. 244–270.
- [17] I. Prigogine, *Etude thermodynamique des phénomènes irréversibles*, Dunod, Paris, (1947).
- [18] S.R. de Groot and P. Mazur, *Non-equilibrium thermodynamics* Dover publications, Inc. New York, 1984.
- [19] J. H. Irving and J. G. Kirkwood, *The statistical mechanics of transport processes. IV. The equations of hydrodynamics*, *J. Chem. Phys.*, 18 (1950), pp. 817–829.
- [20] R. J. Bearman and J. G. Kirkwood, *The statistical mechanics of transport processes. XI. Equations of transport in multicomponent systems*, *J. Chem. Phys.*, 28 (1958), pp. 136–145.
- [21] H. Mori, *Statistical-mechanical theory of transport in fluids*, *Phys. Rev.*, 112 (1958), pp. 1829–1842.
- [22] J. Keizer *Statistical Thermodynamics of Nonequilibrium Processes*, Springer-Verlag, New York, 1987.
- [23] H. Van Beijeren and M. H. Ernst, *The Modified Enskog Equations*, *Phys. A*, 68 (1973), pp. 437–456.
- [24] H. Van Beijeren and M. H. Ernst, *The Modified Enskog Equations for Mixtures*, *Phys. A*, 70 (1973), pp. 225–242.
- [25] V. I. Kurochkin, S. F. Makarenko, and G. A. Tirsikii, *Transport coefficients and the Onsager relations in the kinetic theory of dense gas mixtures*, *J. Appl. Mech. Tech. Phys.*, 25 (1984), pp. 218–225.
- [26] L. J. Gillepsie, *Equilibrium pressures of individual gases in mixtures and the mass-action law for gases*, *J. Am. Chem. Soc.*, 47 (1925), pp. 305–312.
- [27] J. A. Beattie, *The computation of the thermodynamic properties of real gases and mixtures of real gases*, *Chem. Rev.*, 18 (1948), pp. 141–192.
- [28] R.C. Reid, J.M. Prausnitz, B.E. Poling, *The Properties of Gases and Liquids* McGraw-Hill, New-York, (1987).
- [29] A. Ern and V. Giovangigli, *The Kinetic equilibrium regime*, *Physica-A*, 260 (1998), pp. 49–72.
- [30] V. Giovangigli, *Multicomponent flow modeling*, Birkhäuser, Boston, (1999).
- [31] R. Taylor and R. Krishna, *Multicomponent mass transfer*, John Wiley, New York, (1993).
- [32] G. Ribert, M. Champion, O. Gicquel, N. Darabiha, and D. Veynante, *Modeling nonadiabatic turbulent premixed reactive flows including tabulated chemistry*, *Comb. Flame* 141 (2005), pp. 271–280.
- [33] J. Savre, N. Bertier, Y. D'Angelo, and D. Gaffié, *A chemical time scale approach for FPI modeling*, *C. R. Mécanique* 336 (2008), pp. 807–812.

- [34] T. T. H. Verschoyle, *The ternary system Monoxyde-Nitrogen-Hydrogen and the component binary systems between temperatures of -185 degrees and -215 degrees C., and between pressures of 0 and 225 atm*, Phil. Trans. R. Soc. Lond., A230 (1932), pp. 189–220.
- [35] L. S. Eubanks, *Vapor-Liquid equilibria in the system Hydrogen-Nitrogen-Carbon monoxide*, The Rice Institute, Houston, Texas, (1957).
- [36] M. Sermange, *Mathematical and numerical aspects of one-dimensional laminar flame simulation*, Appl. Math. Opt., 14 (1986), pp. 131–153.
- [37] V. Giovangigli and M. Smooke, *Application of continuation techniques to plane premixed laminar flames*, Comb. Sci. and Tech., 87 (1992), p 241–256.
- [38] M. Benedict, G.B. Webb, and L.C. Rubin, *An empirical equation for thermodynamic properties of light hydrocarbons and their mixtures*, J. Chem. Phys. 8 (1940), pp. 334–345.
- [39] G.S. Soave, *An effective modification of the Benedict-Webb-Rubin equation of state*, Fluid Phase Equil. 164 (1999), pp. 157–172.
- [40] O. Redlich and J. N. S. Kwong, *On the thermodynamics of solutions. V An equation of state. Fugacities of gaseous solutions*, Chem. Reviews 44 (1949), pp. 233–244.
- [41] G.S. Soave, *Equilibrium constants from a modified Redlich-Kwong equation of state*, Chem. Eng. Sci. 27 (1972), pp. 157–172.
- [42] D.Y. Peng and D.B. Robinson, *A new two-constant equation of state*, Indus. Eng. Chem. Fund. 15 (1976), pp. 59–64.
- [43] K.G. Harstad, R.S. Miller, and J. Bellan, *Efficient High Pressure State Equations*, AIChE J. 43-6 (1997), pp. 1605–1610.
- [44] A. Congiunti, C. Bruno, and E. Giacomazzi, *Supercritical combustion properties*, in *11th Aerospace Sciences Meeting and Exhibit*, Reno, Nevada, USA, 6–9 January, AIAA-2003-478, 2003.
- [45] P. Colonna and P. Silva, *Dense gas thermodynamic properties of single and multicomponent fluids for fluid dynamics simulations*, J. Fluid Eng. 125 (2003), pp. 414–427.
- [46] W.A. Cañas-Marín, U.E. Guerrero-Aconcha, and J.D. Ortiz-Arango, *Comparison of different cubic equations of state and combination rules for predicting residual chemical potential of binary and ternary Lennard-Jones mixtures: Solid-supercritical fluid phase equilibria*, Fluid Phase Equil. 234 (2005), pp. 42–50.
- [47] W.A. Cañas-Marín, J.D. Ortiz-Arango, U.E. Guerrero-Aconcha, and C.P. Soto-Tavera, *Thermodynamic derivative properties and densities for hyperbaric gas condensates: SRK equation of state predictions versus Monte Carlo data*, Fluid Phase Equil. 253 (2007), pp. 147–154.
- [48] H. Meng and V. Yang, *A unified treatment of general fluid thermodynamics and its application to a preconditioning scheme*, J. Comp. Phys. 189 (2003), pp. 277–304.
- [49] V. Giovangigli and L. Matuszewski, *Supercritical Thermochemistry*, (in preparation)
- [50] L. Waldmann, *Transporterscheinungen in Gasen von mittlerem Druck*, Handbuch der Physik, 12, (1958) 295–514.
- [51] J. Van de Ree, *On the definition of the diffusion coefficients in reacting gases*, Physica, 36 (1967), pp. 118–126.

- [52] S. Chapman and T.G. Cowling, *The mathematical theory of non-uniform gases* Cambridge University Press, Cambridge, 1970.
- [53] C. Eckart, *The thermodynamic of irreversible processes, II. Fluid mixtures*, Phys. Rev., 58 (1940), pp. 269–275.
- [54] K.G. Harstad and J. Bellan, *Mixing rules for multicomponent mixture mass diffusion coefficients and thermal diffusion factors*, J. Chem. Phys. 120-12 (2004), pp. 5664–5673.
- [55] S. Sarman and D. Evans, *Heat flow and mass diffusion in binary Lennard-Jones mixtures*, Physical Review A, 45 (1992), pp. 2370–2379.
- [56] J. O. Hirschfelder, C. F. Curtiss, and R. B. Bird, *Molecular theory of gases and liquids*, Wiley, New York (1954).
- [57] E. D. Ozokwelu and J. H. Erbar, *An improved Soave-Redlich-Kwong equation of state*, Chem. Eng. Comm., 52 (1987), pp. 9–19.
- [58] M. S. Grabovski and T. E. Daubert, *A modified Soave equation of state for phase equilibrium calculations. 3. Systems containing Hydrogen*, Ind. Eng. Chem. Process. Dev. Des., 18 (1979), pp. 300–306.
- [59] M. W. Chase, Jr., *NIST-JANAF thermochemical tables*, Fourth Ed., J. Phys. Chem. Ref. Data, Monograph 9 (1998).
- [60] B. J. McBride, M. J. Zehe, and S. Gordon, *NASA Glenn coefficients for calculating thermodynamic properties of individual species*, NASA/TP–2002-211556 (2002).
- [61] J. Warnatz, *Survey of rate coefficients in the C/H/O system*, in : W. C. Gardiner Ed., *Combustion Chemistry*, Springer, New York (1984), 197–360.
- [62] V. M. Zhdanov, *Transport processes in multicomponent plasmas*, Taylor and Francis, London, (2002).
- [63] J. H. Ferziger and H. G. Kaper, *Mathematical theory of transport processes in gases* North-Holland Publishing Company, Amsterdam, (1972).
- [64] V. Giovangigli, *Convergent iterative methods for multicomponent diffusion*, Impact Comput. Sci. Eng., 3 (1991), pp. 244–276.
- [65] A. Ern and V. Giovangigli, *Multicomponent transport algorithms* Lecture Notes in Physics, Monograph m24, Springer-Verlag, Heidelberg, (1994).
- [66] L. J. T. M. Kempers, *A thermodynamic theory of the Soret effect in a multicomponent liquid*, J. Chem. Phys. 90 (1989), pp. 6541–6548.
- [67] A. Ern and V. Giovangigli, *Thermal diffusion effects in hydrogen-air and methane-air flames*, Comb. Theory Mod. 2-4 (1998), pp. 349–372.
- [68] A. Ern and V. Giovangigli, *Impact of Multicomponent Transport on Planar and Counterflow Hydrogen/Air and Methane/Air Flames*, Comb. Sci. Tech., **149**, (1999) pp. 157–181.
- [69] R. Bendahkia, V. Giovangigli, and D. Rosner, *Soret effects in laminar counterflow spray diffusion flames*, Comb. Theory Mod., 6 (2002), pp. 1–17.
- [70] T.H. Chung, M. Ajlan, L.L. Lee, and K.E. Starling, *Generalized Multiparameter correlation for nonpolar and polar fluid transport properties*, Ind. Eng. Chem. Res., 27 (1988), pp. 671–679.

- [71] J.F. Ely and H.J. Hanley, *Prediction of transport properties. 2. Thermal conductivity of pure fluids and mixtures*, Indus. Eng. Chem. Fund. 22 (1983), pp. 90–97.
- [72] A. Ern and V. Giovangigli, *Thermal conduction and thermal diffusion in dilute polyatomic gas mixtures*, Physica-A, 214 (1995), pp. 526–546.
- [73] A. Laesecke, R. Krauss, K. Stephan, and W. Wagner, *Transport Properties of Fluid Oxygen*, J. Phys. Chem. Ref. Data, 19 (1990), pp. 1089–1122.
- [74] N. B. Vargaftik, *Handbook of physical properties of liquids and gases*, Begell House (New York) 1996
- [75] A. Ern and V. Giovangigli, *Projected iterative algorithms with application to multicomponent transport*, Linear Algebra Appl., 250 (1997), pp. 289–315.
- [76] A. Ern and V. Giovangigli, *Optimized transport algorithms for flame codes*, Comb. Sci. Tech., 118 (1996), pp. 387–395.
- [77] V. Giovangigli, *Multicomponent transport algorithms for partially ionized plasmas*, J. Comp. Phys., 229 (2010), pp. 4117–4142.
- [78] E. S. Oran and J. P. Boris, *Numerical simulation of reactive flows* Cambridge university press, Cambridge, (2001).
- [79] M. D. Smooke, *Solution of burner stabilized premixed laminar flames by boundary value methods*, J. Comp. Phys., 48 (1982), pp. 72–105.
- [80] V. Giovangigli and M. D. Smooke, *Adaptive continuation algorithms with application to combustion problems*, Appl. Numer. Math., 5 (1989), pp. 305–331
- [81] V. Giovangigli V and N. Darabiha, *Vector Computers and Complex Chemistry Combustion, Mathematical Modeling in Combustion and Related Topics* (Brauner C and Schmidt-Laine C Eds. Nijhoff M Pug.) NATO ASI Series, 140 (1988), pp. 491–503.
- [82] A. Ern and V. Giovangigli, *EGLib server and User's manual*, <http://www.cmap.polytechnique.fr/www.eglib>.
- [83] L. Matuszewski, *PhD Thesis*, University Paris 6, (in preparation).
- [84] M. D. Smooke, J. A. Miller, and R. J. Kee, *Numerical solution of burner stabilized premixed laminar flames by an efficient boundary value method*, in Numerical Methods in Laminar Flame Propagation, N. Peters and J. Warnatz eds., Vieweg Verlag, (1982), pp. 112–129.
- [85] J. Warnatz, *Theoretical and numerical combustion*, Springer Verlag, Berlin (1982).
- [86] F. A. Williams, *Combustion theory*, Menlo Park, (1982).
- [87] G. Joulin et P. Clavin, *Analyse Asymptotique des Conditions d'Extinction des Flamme Laminaires*, Acta Astronautica, 3 (1976), pp. 223–240.
- [88] V. Giovangigli V and M. D. Smooke, *Application of Continuation Techniques to Plane Premixed Laminar Flames*, Comb. Sci. Tech., 87 (1992), pp. 241–256.
- [89] R. S. Barlow, A. N. Karpetis, J. H. Frank, and J. H. Chen, *Scalar profiles and NO formation in laminar opposed-flow partially premixed Methane/Air flames*, Comb. and Flame, 127 (2001), pp. 2102–2118.